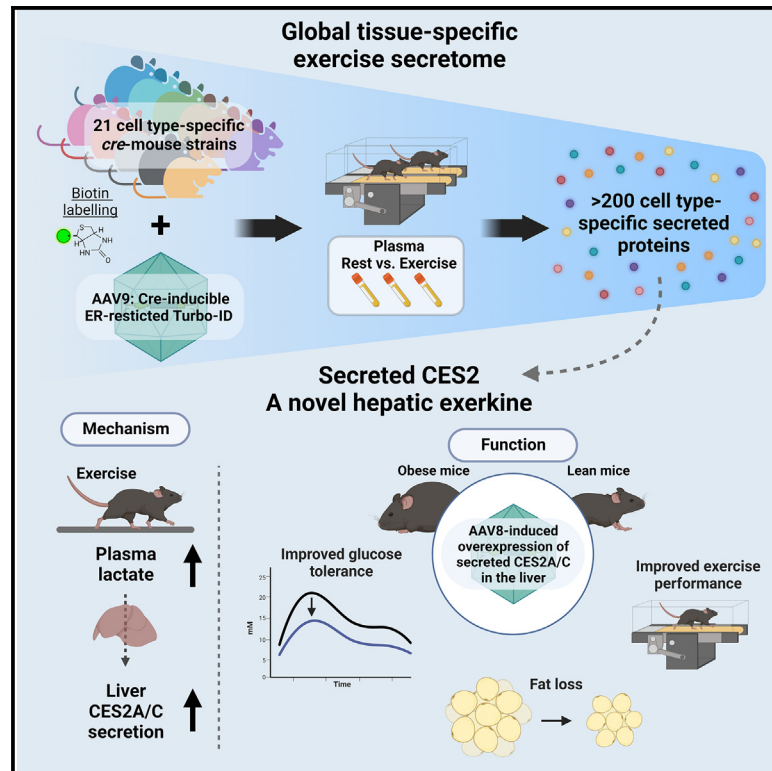


Cell Metabolism

Organism-wide, cell-type-specific secretome mapping of exercise training in mice

Graphical abstract



Authors

Wei Wei, Nicholas M. Riley, Xuchao Lyu, ..., Michael P. Snyder, Carolyn R. Bertozzi, Jonathan Z. Long

Correspondence

jzlong@stanford.edu

In brief

Wei et al. use proteomics to identify cellular secretome changes in response to exercise training at an organism-wide scale. Using this dataset, Wei et al. identified two exercise-inducible secreted proteins from the liver that enhance running performance and improve metabolic health.

Highlights

- An organism-wide cell-type-specific secretome atlas after exercise training in mice
- Exercise training induces cell-type-specific and bidirectional secretome changes
- *Pdgfra*⁺ cells are highly responsive to exercise training
- Secreted CES2 proteins improve metabolic health and enhance running endurance



Resource

Organism-wide, cell-type-specific secretome mapping of exercise training in mice

Wei Wei,^{1,2,3,15} Nicholas M. Riley,^{3,4,5,15} Xuchao Lyu,^{1,3,14,15} Xiaotao Shen,⁶ Jing Guo,⁷ Steffen H. Raun,⁸ Meng Zhao,^{1,9,10} Maria Dolores Moya-Garzon,^{1,3} Himanish Basu,¹¹ Alan Sheng-Hwa Tung,^{1,3} Veronica L. Li,^{1,3,4} Wentao Huang,^{12,13} Amanda L. Wiggenhorn,^{1,3,4} Katrin J. Svensson,^{1,9,10} Michael P. Snyder,^{5,9,10} Carolyn R. Bertozzi,^{3,4,5} and Jonathan Z. Long^{1,3,9,10,14,16,*}

¹Department of Pathology, Stanford University School of Medicine, Stanford, CA 94305, USA

²Department of Biology, Stanford University, Stanford, CA 94305, USA

³Sarafan ChEM-H, Stanford University, Stanford, CA 94305, USA

⁴Department of Chemistry, Stanford University, Stanford, CA 94305, USA

⁵Howard Hughes Medical Institute, Stanford University, Stanford, CA 94305, USA

⁶Department of Genetics, Stanford University School of Medicine, Stanford, CA 94035, USA

⁷Department of Microbiology and Immunology, Stanford University School of Medicine, Stanford, CA 94305, USA

⁸Department of Biomedical Sciences, University of Copenhagen, Copenhagen, Denmark

⁹Stanford Diabetes Research Center, Stanford University School of Medicine, Stanford, CA 94305, USA

¹⁰Cardiovascular Institute, Stanford University School of Medicine, Stanford, CA 94305, USA

¹¹Department of Immunology, Harvard Medical School, Boston, MA 02115, USA

¹²Whitehead Institute for Biomedical Research, Cambridge, MA 02142, USA

¹³Department of Biology, Massachusetts Institute of Technology, Cambridge, MA 02142, USA

¹⁴Wu Tsai Human Performance Alliance, Stanford University, Stanford, CA 94305, USA

¹⁵These authors contributed equally

¹⁶Lead contact

*Correspondence: jzlong@stanford.edu

<https://doi.org/10.1016/j.cmet.2023.04.011>

SUMMARY

There is a significant interest in identifying blood-borne factors that mediate tissue crosstalk and function as molecular effectors of physical activity. Although past studies have focused on an individual molecule or cell type, the organism-wide secretome response to physical activity has not been evaluated. Here, we use a cell-type-specific proteomic approach to generate a 21-cell-type, 10-tissue map of exercise training-regulated secretomes in mice. Our dataset identifies >200 exercise training-regulated cell-type-secreted protein pairs, the majority of which have not been previously reported. *Pdgfra*-cre-labeled secretomes were the most responsive to exercise training. Finally, we show anti-obesity, anti-diabetic, and exercise performance-enhancing activities for proteoforms of intracellular carboxylesterases whose secretion from the liver is induced by exercise training.

INTRODUCTION

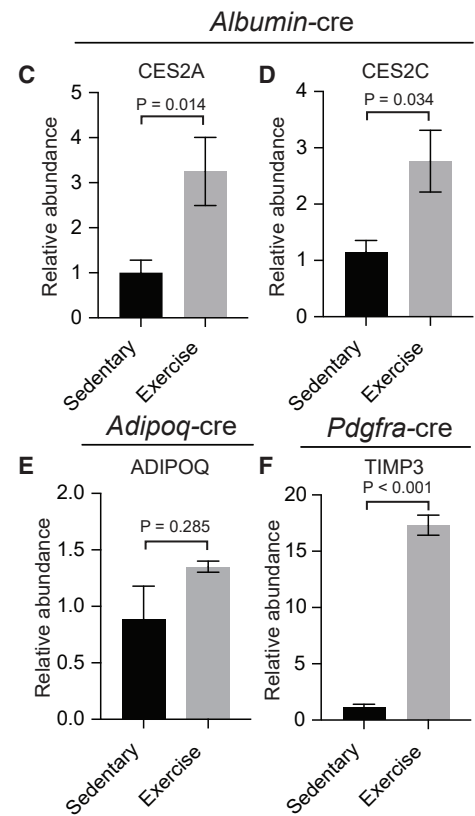
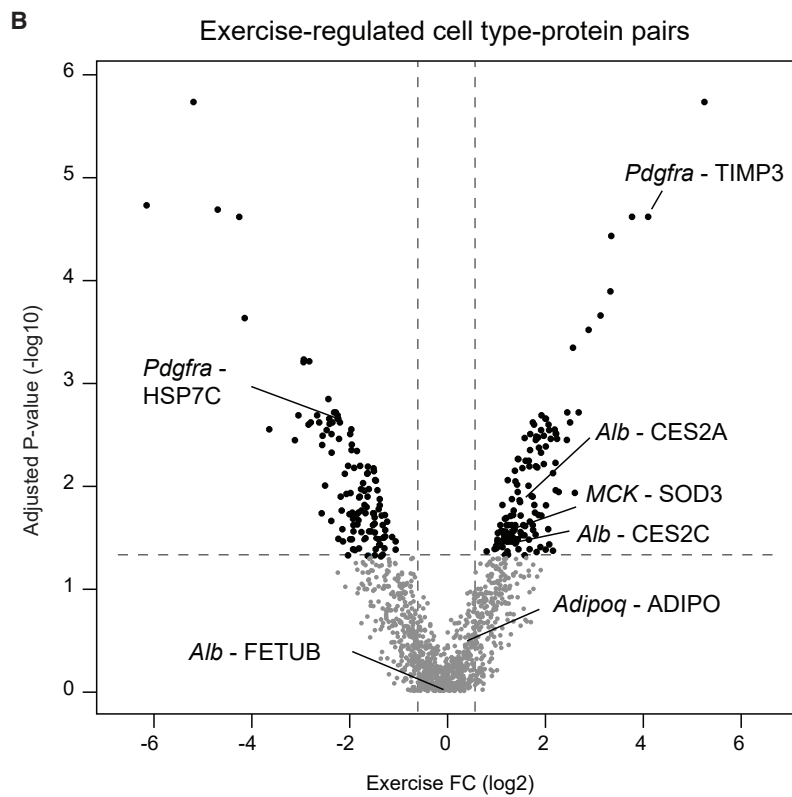
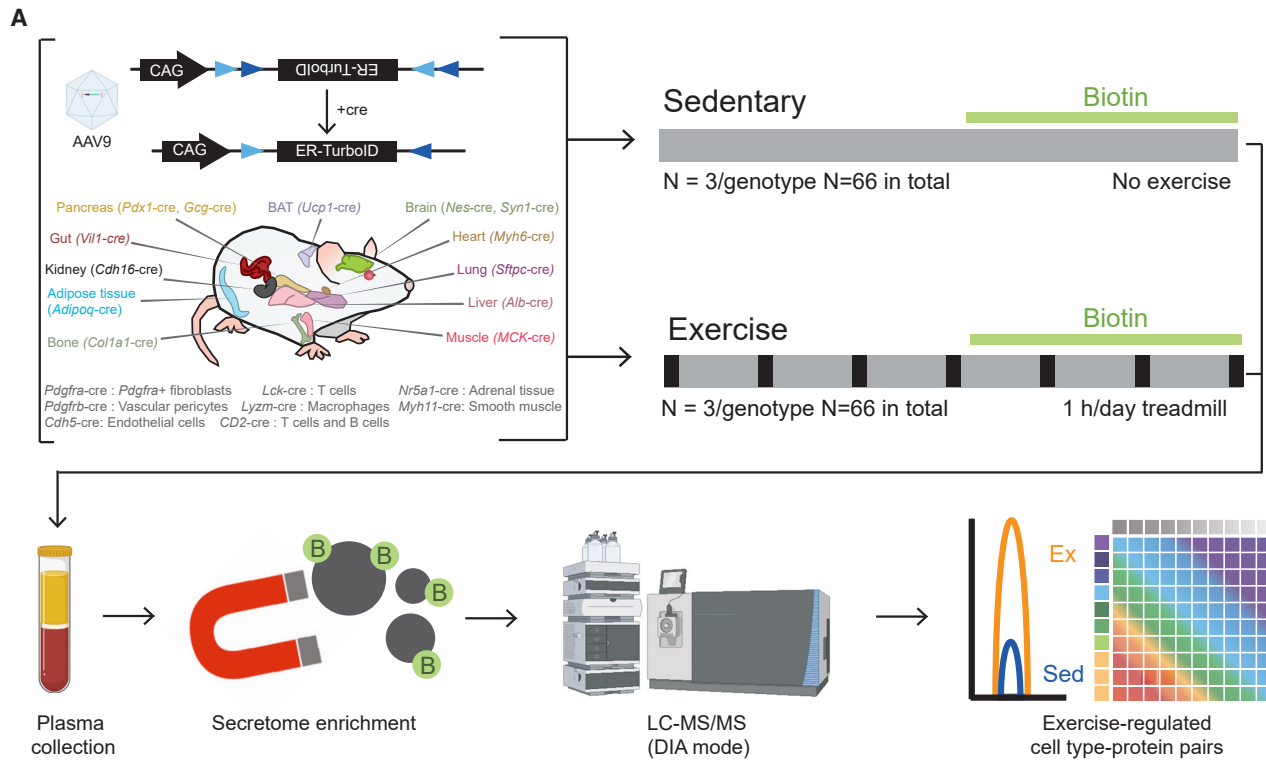
Physical activity is a powerful physiologic stimulus that provides benefits to many organ systems and confers protection against disease.^{1,2} Conversely, physical inactivity is a major contributor to cardiovascular morbidity and mortality.^{3,4} The magnitude of the benefits of physical activity is comparable, and in some cases even greater, than currently available first-line pharmacological treatments.^{5–7} The mechanisms responsible for the benefits of exercise are incompletely understood, but likely extend beyond activity-associated increases in energy expenditure alone.^{8,9}

In recent years, there has been tremendous interest in the identification and characterization of exercise-inducible, soluble (e.g., secreted) blood-borne molecules. These circulating mole-

cules, which have been called “exerkines” or “exercise factors,” are secreted signaling molecules that function as molecular effectors of physical activity.^{10,11} Over 50 years ago, Goldstein¹² demonstrated that contracting muscle from dogs produced a humoral factor that stimulated glucose uptake when transferred to non-exercised muscle preparations. More recently, experiments involving re-infusion of exercise-conditioned plasma in mice have also provided additional evidence for bioactive molecules present in the circulation following exercise.^{13,14}

At a molecular level, many individual candidate metabolites, lipids, polypeptides, and proteins have been proposed to function as exerkines.^{15–24} However, these previous efforts have typically focused on a single factor (e.g., IL-6) and/or a single cell type/tissue of origin (e.g., muscle). Few studies have systematically mapped exercise-inducible secreted molecules across an





(legend on next page)

entire organism. A major challenge, especially for secreted polypeptides and proteins, has been the low depth of plasma proteome coverage by classical shotgun proteomics techniques.²⁵ Aptamer- and antibody-based approaches provide higher sensitivity but are not comprehensive for the plasma proteome and cannot be used to detect the array of potentially new proteoforms or cleavage fragments that might be produced following physical activity.^{17,26} Finally, many secreted proteins are expressed by multiple cell types, and single snapshot detection of these molecules in the circulation would not be expected to enable detection of cell-type-specific and potentially complex regulation of exercise-inducible changes across distinct cell types.

We^{27,28} and others^{29–31} have recently described a biochemical secretome profiling methodology that enables direct labeling, enrichment, and identification of secreted proteins in mice at a cell-type-specific resolution. Key to this methodology is the delivery of an engineered biotinylation enzyme TurboID³² into the secretory pathway of cells via adeno-associated virus (AAV) transduction. Cell-type-specific labeling is achieved genetically because the expression of the TurboID is restricted to those cells expressing cre recombinase. Biotinylated and secreted plasma proteins can then be purified directly from blood plasma using streptavidin beads and analyzed by liquid chromatography-tandem mass spectrometry (LC-MS/MS). Our initial secretome studies with the proximity biotinylation approach previously established that cell-type-specific secretome changes could be profiled directly in an intact animal.²⁸ Here, we have extended this secretome profiling to organism-wide scale and examined the cell-type-specific secretome response to exercise training. Our organism-wide 21-cell-type, 10-tissue secretome map of physical activity provides fundamental insights into the molecular identity and cellular origin of exercise training-regulated circulating factors and illuminates the dynamic regulation of intercellular and inter-organ crosstalk by physical activity.

RESULTS

Study design and proteomic map of exercise training-regulated secretomes

The experimental design for organism-wide, cell-type-specific secretome profiling in response to exercise training is shown schematically in Figure 1A. First, we generated AAV serotype 9 (AAV9) expressing a cre-inducible, endoplasmic reticulum-restricted TurboID (AAV9-FLEEx-ER-TurboID, 3×10^{11} GC/mouse, intravenously) (Figure 1A; STAR Methods). In cells expressing cre recombinase, inversion of the FLEEx cassette results

in robust expression of the ER-TurboID construct. AAV9 was chosen since this serotype exhibits broad tissue distribution and transduction.³³ Next, we assembled 21 manually curated hemizygous cre mouse driver lines from the Jackson Laboratories ($n = 6$ /genotype; Figure 1A; STAR Methods). Included among the set of cre driver lines were those that target specific organs previously shown to participate in response to exercise training (e.g., *MCK*-cre targeting muscle, *Adiponectin*-cre targeting fat, and *Albumin*-cre targeting liver). Other cre drivers exhibited well-validated expression patterns (e.g., *Lysm*-cre for macrophages), even though those cell types had not been previously implicated in the response to physical activity. In the cases where tamoxifen-inducible cre driver lines were used, tamoxifen (2 mg/mouse, intraperitoneally) was administered 2 weeks after viral transduction. As expected, robust *TurboID* mRNA expression was detected in tissues from all transduced mice compared to virally transduced, wild-type control mice (Figure 1A; STAR Methods). Furthermore, we harvested a collection of tissues from a subset of cre driver mice in which TurboID expression was predicted to occur in an organ-restricted manner (*Albumin*-cre for liver, *Ucp1*-cre for brown fat, *Adiponectin*-cre for all adipose, *MCK*-cre for muscle, *Myh6*-cre for heart, *Pdx1*-cre for pancreas, and *Syn1*-cre for brain). V5-tagged TurboID protein, as measured by western blot using an anti-V5 epitope tag antibody, was robustly detected with the expected organ-restricted pattern (Figure S1B).

Given the expansive scope of our initial proteomic survey, we reasoned that performing our initial proteomic studies in a single sex would be the most reasonable approach and most useful for downstream data analysis. Male mice were virally transduced for 3 weeks to allow for robust TurboID expression across cell types. Then mice were separated into treadmill running or sedentary groups ($n = 3$ per group per genotype; Figure 1A). Our 1-week treadmill running protocol, adapted from Wu et al.,³⁴ consisted of running for 60 min/day at a speed of 20 m/min. To control for potential perturbations of circadian rhythms, control sedentary mice were also transferred to the same room as the exercise training animals (STAR Methods). After the 1-week treadmill training protocol, mRNA levels of *Pgc1a* and *Nr4a1* in quadriceps muscle were consistently induced by on average 1.6-fold and 1.3-fold, respectively, across all animals (Figures S1C and S1D).^{35–37} Total inguinal white adipose tissue mass was reduced by 30% in the exercise group (sedentary, 333 ± 11 mg; exercise, 237 ± 11 mg; mean \pm SEM, $p < 0.001$) (Figure S1E). Histological analysis of the inguinal adipose tissue also showed reduced adipocyte size (Figure S1F). Additionally, exercised animals of all genotypes exhibited -0.68 ± 0.02 g (mean \pm SEM, $n = 66$)

Figure 1. Study design and overview of exercise training secretomes across 21 cell types in mice

(A) Overview of the study design including viral transduction (AAV9-FLEEx-ER-TurboID, 3×10^{11} GC/mouse, intravenously) of 21 cre driver lines (male, $n = 3$ /condition/genotype; STAR Methods) and wild-type C57BL/6 mice (male, $n = 3$ /condition), 1-week treadmill running (20 m/min for 60 min per day), secretome labeling (biotin delivered via 0.5 mg/mL biotin water and via injection [24 mg biotin/mL, intraperitoneally, in a solution of 18:1:1 saline:Kolliphor EL:DMSO, final volume of 200 μ L per mouse per day] in the last 3 days of running), enrichment of biotinylated plasma proteins using streptavidin beads, and proteomic analysis. BAT, brown adipose tissue.

(B) Volcano plot of adjusted p values ($-\log_{10}$) and exercise fold change (\log_2) of a total of 1,272 cell type-protein pairs. Adjusted p values were calculated from moderated t-statistics (STAR Methods). Black dots indicate exercise-regulated cell type-protein pairs (adjusted $p < 0.05$ and exercise fold change > 1.5) and gray dots indicate unchanged cell type-protein pairs (adjusted $p > 0.05$ or exercise fold change < 1.5).

(C–F) Relative abundance of exercise training-regulated (C, D, and F) and exercise training-unregulated (E) cell type-protein pairs from exercise and sedentary mice. $n = 3$ /genotype/condition, mean \pm SEM. p values were calculated from two-tailed unpaired t tests.

weight change during the 1-week treadmill running, whereas the sedentary controls ($n = 66$) gained $+0.50 \pm 0.02$ g (mean \pm SEM, $n = 66$; Figure S1G). This body weight difference was in part due to slightly reduced food intake (Figure S1H). Taken together, these molecular and physiologic data validate both the secretome labeling mouse lines as well as the 1-week exercise training protocol.

To determine the identity of exercise training-regulated secreted proteins and their cell types of origin, we supplemented biotin to mice for the final 3 days of the exercise training protocol to biotinylate *in vivo* secretomes (Figures 1A, right, and S1; STAR Methods). Two hours after the final bout of running, blood plasma was collected from each mouse and biotinylated secreted proteins were purified using streptavidin beads, digested following an S-trap protocol, and analyzed by LC-MS/MS in data-independent acquisition (DIA) mode (STAR Methods). We chose to use a previously described spectrum library-free DIA approach that relies on gas-phase fractionation (GPF)-DIA data from a pooled sample to generate DIA-only chromatogram libraries.^{38,39} This allowed us to search all data against experiment-specific chromatogram libraries using the freely available EncyclopeDIA platform,³⁸ followed by further processing in the Skyline and Perseus data analysis environments.^{40,41} Because our dataset provides information about both secreted proteins and cell types, we define a “cell type-protein pair” as a set [protein, cell type], which indicates the detection of that secreted protein in the indicated cell type secretome. To filter for bona fide cell type-protein pairs enriched by streptavidin, we also applied a 1.5-fold enrichment filter for each cell type-protein pair versus non-transduced, wild-type controls (STAR Methods). In total across all samples ($n = 3$ mice/condition \times 2 conditions \times 21 genotypes), we detected 1,272 unique cell type-protein pairs with ≥ 2 peptides detected in all 3 replicates of both conditions (Table S1).

Exercise training-regulated cell type-protein pairs were identified by comparison of differential secreted proteins from the same cell type in sedentary versus exercised mice. This comparison also provides a natural control for differing levels of proximity labeling enzyme expression and/or varying levels of secretome biotinylation between distinct cell types. Exercise training significantly altered 256 cell type-protein pairs consisting of 181 unique proteins changed across 21 cell types (20.1% of the entire dataset, adjusted $p < 0.05$ and exercise fold change > 1.5 ; Figure 1B; Table S1), many of which have not been previously described. Fewer unique proteins ($n = 181$) than all exercise training-regulated cell type-protein pairs ($n = 256$) were observed because the same protein can be secreted by more than one cell type. We identified several example candidates of exercise training-regulated secreted proteins selectively altered in one cell type (Figures 1C–1F). For instance, two carboxylesterases, CES2A and CES2C, were increased by 3-fold exclusively in secretomes from *Albumin-cre* mice following treadmill running (Figures 1C and 1D). CES2 enzymes are classically annotated as intracellular, liver-enriched endoplasmic reticulum resident proteins. Nevertheless, our data suggest that CES2 enzymes can also be released from the liver in an exercise training-dependent manner. Other well-established secreted protein-cell type pairs, such as the hormone adiponectin from fat cells (ADIPOQ in *Adipoq-cre* transduced secre-

tores),⁴² were robustly detected in our dataset but not regulated by physical activity (Figure 1E). Finally, one of the most exercise training-inducible cell type-protein pairs in the dataset was TIMP3 from *Pdgfra-cre*-labeled secretomes (Figure 1F). While TIMP3 had previously been implicated in diverse physiologic roles including in myogenesis,⁴³ thermogenesis and metabolism,⁴⁴ vascular remodeling,⁴⁵ and atherogenesis,⁴⁶ its exercise training-inducible secretion from *Pdgfra-cre*-labeled cells has not been previously identified. We conclude that 1 week of treadmill running in mice results in specific modulation of a subset of secreted protein-cell type pairs across our entire secretome dataset.

Systematic analysis of exercise training-regulated cell type-secreted protein pairs

The distribution of these exercise training-regulated cell type-protein pairs across the 21 cell types is shown in Figure 2A. We observed an average and median of 12 and 10, respectively, proteins changed per cell-type secretome in response to exercise training, with a range across all cell types of 1–44. The number of proteins changed in each cell-type secretome by exercise training was not simply correlated with secretome size since the two cell types with the largest number of unique proteins identified in their secretomes (*Albumin-cre*, with 142 proteins, and *MCK-cre*, with 132 proteins) exhibited near the median number of exercise training-regulated secreted protein changes (Figure 2A). All cell types exhibited some secretome changes following exercise training, demonstrating that all cell types exhibit exercise training responsiveness to some degree as measured by changes to their production of soluble factors. Approximately half of the exercise training-regulated secretome changes (50%, 129 out of 256) were observed in only one cell type (Figure 2B). In addition, the frequency of either exercise training up- or downregulated proteins was equivalent (66 proteins increased and 63 proteins decreased; Figure 2B), suggesting that exercise training regulation of soluble factors does not only involve production of new secreted molecules, but also suppression and other regulation of active protein secretion. The other half of the exercise training-regulated secretome changes (50%, 127 out of 256) were proteins expressed in multiple cell types that exhibited cell-type-specific regulation following exercise training. In this latter group, bidirectional change, defined as upregulation in one cell type and downregulation in a different cell type, was commonly observed (40%). These data further underscore the increased resolution afforded by cell-type-specific secretome profiling, as well as the need to use global approaches for evaluating exercise training-induced changes, which are complex, bidirectional, and cell-type specific.

For proteins that were secreted by more than one cell type, we also observed interesting patterns of cell-type-specific responses to exercise training (Figures 2C–2F). For instance, LOXL1, a secreted enzyme involved in extracellular protein lysine oxidation, was selectively downregulated following exercise training in secretomes from *Pdgfra-*, *Nr5a1-*, and *Lysm-cre* transduced mice (Figure 2C). Conversely, the extracellular matrix protein EMIL1 was upregulated following exercise training selectively in *Col1a1-*, *Lysm-*, and *Nr5a1-cre* secretomes (Figure 2D). We also identified several examples of proteins expressed in multiple cell types and bidirectionally regulated by exercise

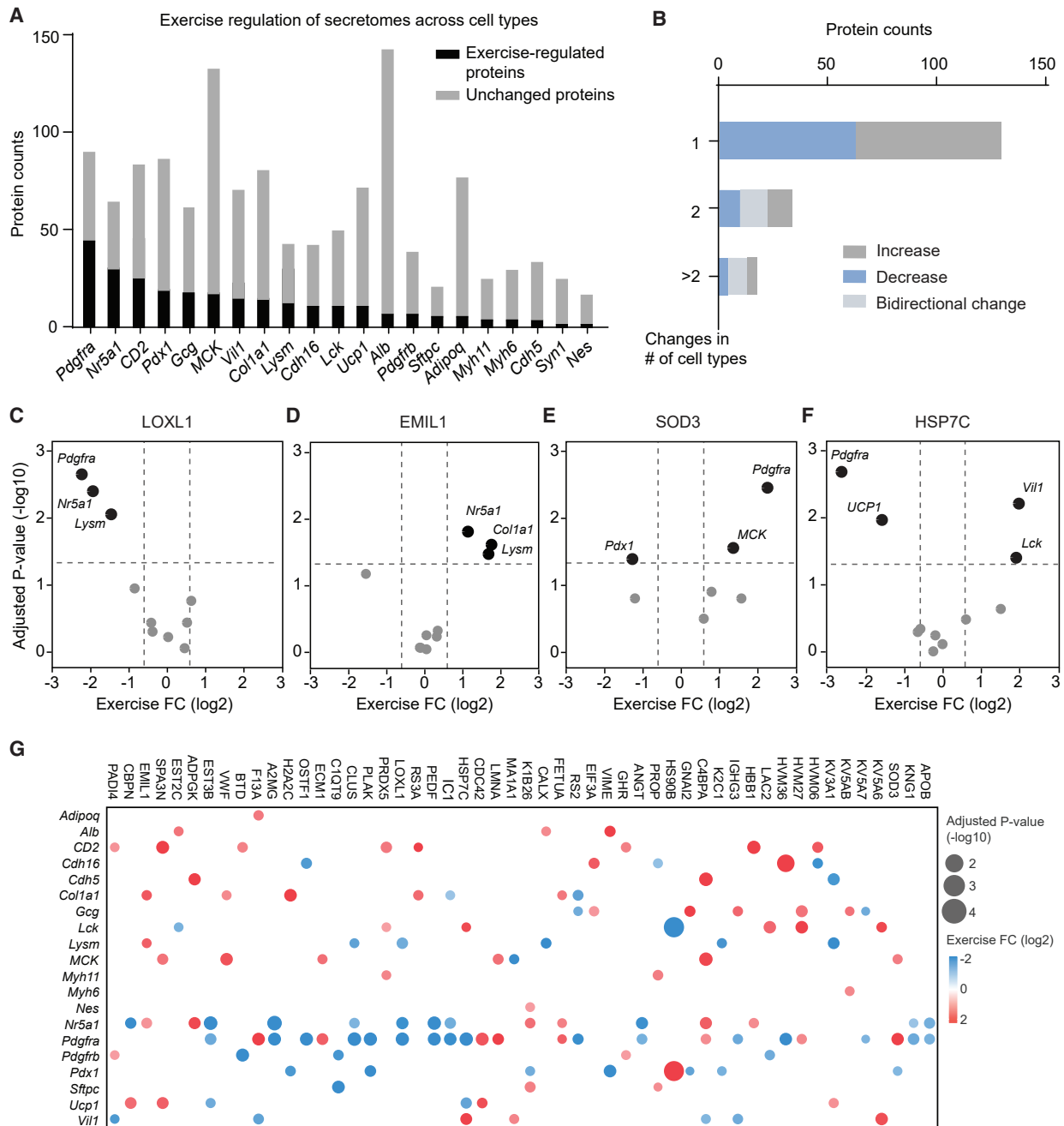


Figure 2. Systematic analysis of exercise training-regulated cell type-protein pairs

(A) Bar graph of exercise training-regulated proteins (black) and unchanged proteins (gray) across 21 cell types.

(B) Histogram of increased (gray), decreased (blue), and bidirectionally changed (light gray) secreted proteins after exercise training across 21 cell types.

(C–F) Volcano plot of adjusted p values ($-\log_{10}$) and exercise fold change (\log_2) of indicated example proteins. Black dots indicate exercise training-regulated cell type-protein pairs (adjusted $p < 0.05$ and exercise fold change > 1.5) and gray dots indicate unchanged cell type-protein pairs (adjusted $p > 0.05$ or exercise fold change < 1.5).

(G) Bubble plot of adjusted p values ($-\log_{10}$) and exercise fold change (\log_2) of proteins changed in more than 1 cell type after exercise training. Red dots indicate increased proteins after exercise training and blue dots indicate decreased proteins.

training. These include SOD3 (upregulated in *MCK*-cre and *Pdgfra*-cre and downregulated in *Pdx1*-cre secretomes) (Figure 2E) and HSP7C (upregulated in *Vil1*-cre and *Lck*-cre and downregulated in *Pdgfra*-cre and *UCP1*-cre secretomes) (Fig-

ure 2F). A bubble plot visualizing all such examples of exercise training-regulated secreted proteins with regulation ≥ 2 secretomes is shown in Figure 2G. While several of these proteins have been identified as exercise training-regulated proteins in

the literature, our dataset further contextualizes and refines their interpretations at a cell-type level. For instance, total plasma SOD3 was previously reported to be induced by acute treadmill running in humans as well as voluntary wheel running and treadmill exercise training in mice.^{47–50} However, only one of these previous studies suggested that muscle is a cellular origin for exercise training-inducible SOD3.⁴⁸ Our dataset not only confirms upregulation of SOD3 secretion from muscle following exercise training, but also identifies *Pdgfra* and *Pdx1* as additional cell types that express SOD3 and contribute to the exercise training-inducible regulation of this protein (Figure 2E). Similarly, PEDF is a neurotrophic growth factor widely expressed across multiple cell types. In humans, circulating PEDF is reduced after a single bout of cycling⁵¹ as well as after 12-month moderate-intensity aerobic exercise training.⁵² PEDF was downregulated in our dataset in both *Nr5a1*-cre and *Pdgfra*-cre secretomes (Figure 2G), suggesting that these two cell types contribute to the downregulation of plasma PEDF after exercise training. Finally, we manually queried each of the proteins changed in at least one cell type in our study (in total 181 proteins) for any prior knowledge of exercise training regulation. Only ~24% of these factors were known to be regulated by exercise training, and 6 of such proteins had clear cell type/tissue of origin (Table S2). Collectively, our dataset provided more than 200 previously unknown cell type-secreted protein pairs that are under exercise training regulation.

Secretomes from *Pdgfra*-cre-labeled cells are highly responsive to exercise training

While metabolic cell types (muscle, liver, and fat) have typically been examined in the context of exercise training, our dataset indicated that *Pdgfra*-cre-labeled secretomes were among the most exercise training-responsive, as measured by the number of exercise training-regulated proteins (Figure 2A). As an alternative method for determining magnitude of the exercise training response, we also developed a direct “exercise training-responsiveness” metric for each cell-type secretome in our dataset (STAR Methods). This metric takes into account magnitude and statistical significance of the exercise training-regulated changes, as well as the secretome size of that cell type. *Pdgfra*-cre-labeled secretomes once again emerged as the most responsive cell type (exercise training-responsiveness score = 115.4; Figure 3A).

Pdgfra-cre-labeled cells are a population of anatomically distributed cells that have been described in the literature as fibroblasts, mesenchymal stem cells, or progenitor/precursor cells.^{53–55} They have diverse roles in tissue remodeling, fibrosis, and cell proliferation depending on the resident tissue and physiological context.^{53,54} To understand the organ localization of the *Pdgfra*-cre-labeled cells labeled in our secretome labeling experiments, we measured *TurboID* mRNA across multiple tissues from *Pdgfra*-cre transduced mice (Figure S2A). Robust *TurboID* mRNA enrichment was detected across many tissues examined, including lung, adipose tissues (inguinal and brown), muscle, gut, kidney, and brain (Figure S2A). This distribution is similar to the reported expression of *Pdgfra* mRNA across tissues and suggests that *Pdgfra* localized to multiple organs are participating in the exercise training-regulated secretome response detected in our dataset (Figure S2B).

The entire secretome of *Pdgfra*-cre-labeled cells is shown in Figure 3B. A diverse array of secreted proteins with pleiotropic physiologic functions was found to be regulated by exercise training. Some of the most upregulated molecules included the previously mentioned TIMP3 (17-fold) and SOD3 (5-fold), as well as the S100 family member S10AB (5-fold), the HDL-binding protein VIGLN (4-fold), and the vitamin B12 transport protein TCO2 (3-fold). Conversely, downregulated secreted proteins in the *Pdgfra*-cre secretome included ER-resident proteins such as the protein disulfide isomerase PDIA4 (87% suppression) and ER calcium ATPase AT2A3 (88% suppression), the growth factor PEDF (81% suppression), and the lipid metabolizing enzyme PAFA (69% down). Gene ontology analysis revealed enrichment of several biological pathways in the exercise training-regulated *Pdgfra*-cre secretome, of which the highest scoring by gene ratio was “response to stimulus” ($p = 4.96e-07$, gene ratio = 0.77; Figure 3C). Additional biological processes identified from the *Pdgfra*-cre secretome included “response to stress” ($p = 2.00e-06$, gene ratio = 0.45), and “response to organic substance” ($p = 1.03e-04$, gene ratio = 0.34) (Figure 3C). These observations suggest that *Pdgfra*-cre-labeled cells respond to exercise training by sensing exercise training-regulated environmental cues, such as metabolites, cytokines, or other signaling molecules, that in turn drive bidirectional changes in the *Pdgfra*-cre-labeled secretome.

We next sought to validate some of the *Pdgfra*-cre secretome responses using an orthogonal method, as well as to determine whether the secretome changes of *Pdgfra*-labeled cells are dependent on the duration of training. To this end, we used western blotting with commercially available antibodies to determine the levels of three exercise-regulated secreted proteins (F13A, C4BPA, and ITIH2) from the *Pdgfra*-cre secretome in a new cohort of virus-transduced *Pdgfra*-cre mice. In our original proteomic dataset, F13A, C4BPA, and ITIH2 were found to be 4-, 2-, and 4-fold upregulated in *Pdgfra*-cre secretomes after 1 week of treadmill running. In this time course experiment, transduced animals ($n = 3/\text{group}$) were separated into four groups: sedentary, acute exercise (single treadmill bout, 20 m/min for 60 min), or 3-day or 7-day exercise training (daily treadmill running, 20 m/min for 60 min) (Figure 3D). As shown in Figures 3E and S2C, western blotting revealed that all three proteins were robustly elevated from 7-day treadmill running cohorts. Interestingly, while ITIH2 exhibited a similar-magnitude upregulation after 1-day, 3-day, and 7-day running, the upregulation of F13A was specific to 7-day running. On the other hand, C4BPA was downregulated at both 1-day and 3-day treadmill running and upregulated in the 7-day group, indicating this protein is suppressed after acute exercise but increased after chronic training (Figures 3E and S2C). These data demonstrate that the exercise training-regulated proteins in the *Pdgfra*-cre secretome are robust across multiple cohorts and are dependent on the frequency of exercise training.

Finally, we sought to determine potential sex-dependent responses in the *Pdgfra*-cre-labeled secretome. A new cohort of female *Pdgfra*-cre mice was transduced with TurboID virus (AAV9-FLEX-ER-TurboID, 3×10^{11} GC/mouse, intravenously) and secretomes were profiled by shotgun proteomics as described above. Interestingly, *Pdgfra*-cre male and female secretomes exhibited both overlapping and distinct exercise

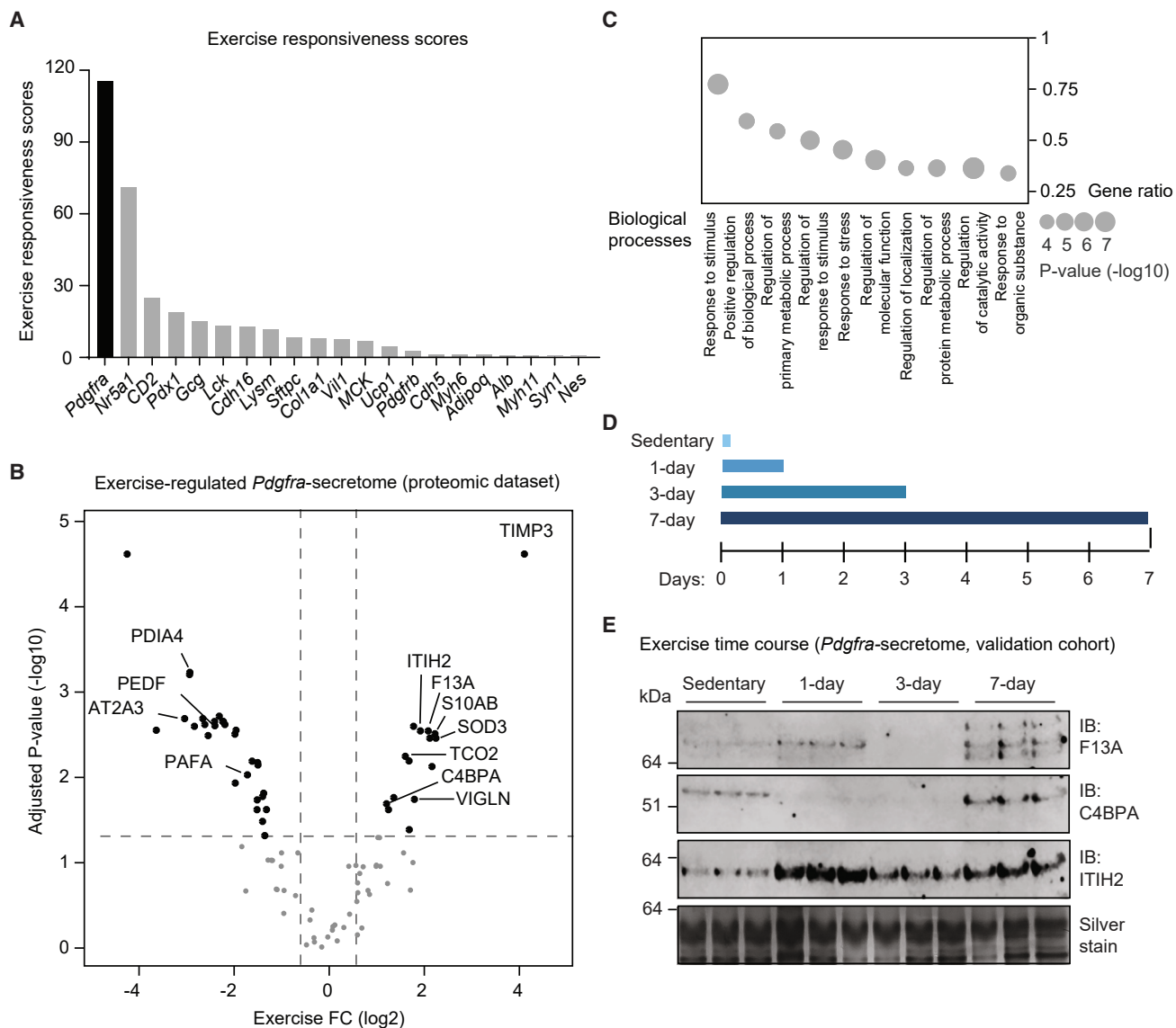


Figure 3. Characterizations of exercise training secretomes from *Pdgfra*-cre-labeled cells

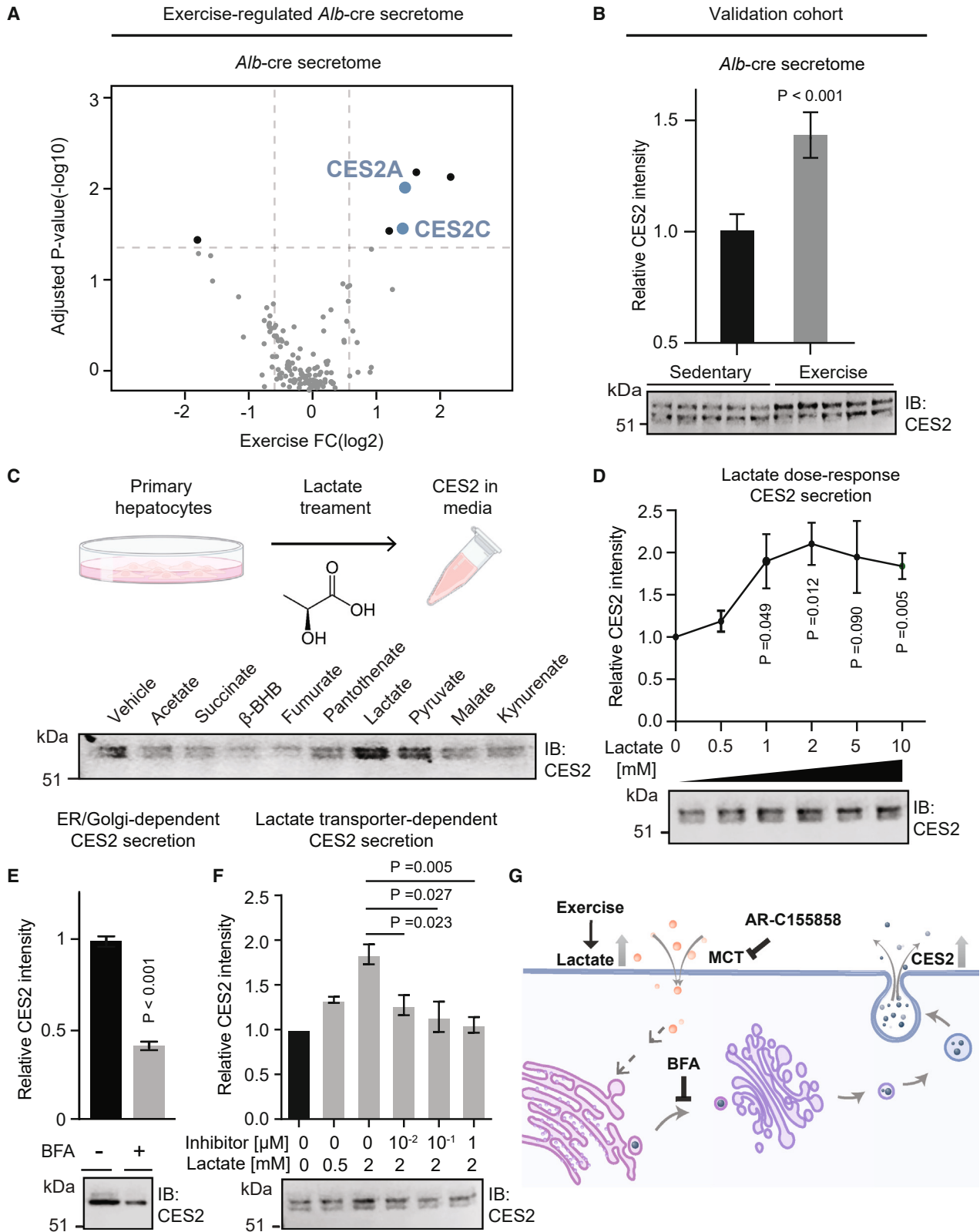
(A) Bar graph of exercise responsiveness scores across cell types. Exercise responsiveness scores of a given cell type were calculated by summarization of the score of individual exercise-regulated protein (adjusted $p < 0.05$ and exercise fold change > 1.5) of that cell type with the following equation: $\text{sum}(\text{absolute exercise fold change} (\log_2) \times \text{confidence of the change} (-\log_{10}(\text{adjusted } p \text{ values}))) \times \text{percent of secretome change} (\text{number of exercise training regulated proteins} (\text{adjusted } p < 0.05 \text{ and exercise fold change } > 1.5) / \text{total number of secreted proteins of that cell type})$. See also [STAR Methods](#).

(B) Volcano plot of adjusted p values ($-\log_{10}$) and exercise fold change (\log_2) of *Pdgfra* secretomes. Black dots indicate exercise training-regulated cell type-protein pairs (adjusted $p < 0.05$ and exercise fold change > 1.5) and gray dots indicate unchanged cell type-protein pairs (adjusted $p > 0.05$ or exercise fold change < 1.5).

(C) Gene ontology analysis of exercise training-regulated proteins (adjusted $p < 0.05$ and exercise fold change > 1.5) from *Pdgfra* secretomes. Size of bubbles represents p values ($-\log_{10}$) of biological process enrichment and y axis represents gene ratio.

(D) Study design of secretome analysis of heterozygous *Pdgfra*-cre mice (12-week-old male, $n = 3/\text{condition}$) injected with 3×10^{11} GC/mouse AAV9-FLEX-ER-TurboID and tamoxifen. Three weeks after tamoxifen delivery, these mice were subjected to acute running (single bout, 20 m/min for 60 min), 3-day or 7-day treadmill running (daily, 20 m/min for 60 min), or being sedentary. Secretome labeling was initiated via injection (24 mg biotin/mL, intraperitoneally, in a solution of 18:1:1 saline:Kolliphor EL:DMSO, final volume of 400 μL per mouse per day) in the last bout of running and biotinylated plasma proteins were enriched using streptavidin beads and analyzed by western blotting ([STAR Methods](#)).

(E) Anti-F13A (top), anti-C4BPA (second row), and anti-ITIH2 (third row) of eluted biotinylated plasma proteins from streptavidin beads after immune purification. Silver stain of total eluted biotinylated plasma proteins was used as loading control and for quantifications (bottom row). Samples ($n = 3/\text{condition}$) were from the experiment described in (D).



(legend on next page)

training responses (Figures S2D and S2E; Table S3). For instance, the sex-independent exercise training-responsive proteins once again included the dramatic elevations in both TIMP3 and F13A (13- and 5-fold increase, respectively) and strong suppression of PEDF, CLUS, and LOXL1 (83%, 73%, and 34% reduction, respectively). Sex-dependent *Pdgfra*-cre secretome changes included induction of VWF only in females (20-fold) and induction of ITIH2 only in males (4-fold). We conclude that sex influences the *Pdgfra*-cre-labeled secretome response to exercise training.

In vitro studies of lactate-stimulated protein secretion

Two of the most robust exercise training-inducible molecules from the *Albumin*-cre-labeled secretome belonged to the same family of carboxylesterase enzymes (CES2A and CES2C; Figure 4A). Because hepatocytes can be easily cultured and manipulated *in vitro*, we used the *Albumin*-cre/CES2 cell type-protein pair as a representative molecular handle to investigate the molecular drivers of this process *in vitro*.

To first validate the exercise training-inducible secretion of CES2 proteins from the liver, we used a commercially available pan-anti-CES2 antibody to probe streptavidin-purified blood plasma from a separate cohort of TurboID-transduced and exercise-trained *Albumin*-cre mice. This commercially available anti-CES2 antibody exhibited the expected immunoreactivity to purified, recombinantly produced CES2A and CES2C proteins (Figure S3A). As expected, extracellular CES2 levels from streptavidin-purified *Albumin*-cre secretomes were increased after exercise training (Figure 4B). The total hepatocyte secretome biotinylation signal remained unchanged (Figure S3B), establishing equivalent secretome protein loading. We therefore conclude that CES2 secretion from the liver is a robust molecular event in response to 1 week of treadmill running.

We sought to test the hypothesis that lactate might serve as an exercise training-inducible extracellular signal that stimulates CES2 secretion from hepatocytes. This hypothesis was based on the well-established increase in lactate flux through the liver via the Cori cycle, as well as our previous experiments showing that other metabolic fuels (e.g., fatty acids) can stimulate protein secretion from the liver.²⁸ We also confirmed that circulating lactate level was increased 3-fold in mice subjected to our 1-week treadmill running protocol compared to sedentary controls (n = 5/condition) (Figure S3C). To test this lactate regulator hypothesis, primary hepatocytes were treated with lactate (2 mM, 4 h) and extracellular CES2 proteins were measured by western blotting in both cell lysates and conditioned medium.

As additional controls, we tested a variety of other exercise training-regulated organic acids, including pyruvate, acetate, malate, fumarate, beta-hydroxybutyrate, kynurenate, and pantothenate.^{20–22,56,57} As shown in Figure 4C, lactate treatment robustly increased the levels of extracellular CES2. Pyruvate, a structurally similar metabolite, also increased CES2 secretion, though with a slightly lower magnitude than that of lactate. By contrast, none of the other metabolites tested increased extracellular CES2 levels (Figures 4C and S3D), establishing that only extracellular lactate, and to a lesser extent pyruvate, exhibit CES2 secretion stimulatory activity.

A dose response of lactate revealed increased CES2 secretion at >1 mM lactate levels (Figure 4D), whereas intracellular CES2 levels were unchanged at all concentrations of lactate tested. In addition, the effect of lactate to induce secretion of CES2 was specific since extracellular albumin levels were unchanged with lactate treatment (Figure S3E). This lactate-induced CES2 secretion is cell-type specific since exogenous expression of CES2A in HEK293T cells resulted in complete retention of this protein intracellularly and treatment of lactate (1–50 mM, 4 h) concentration did not induce the release of CES2A into conditioned medium (Figure S3F). Reduced CES2 secretion was observed when hepatocytes were concurrently treated with lactate (2 mM, 4 h) and an inhibitor of vesicle transport, brefeldin A (BFA; 5 μg/mL, 4 h), establishing that these CES2 proteins are released extracellularly via the classical secretory pathway (Figures 4E and S3G). Last, because lactate import into hepatocytes is critical for this metabolite to function as a substrate in the Cori cycle, we next tested whether lactate import via the monocarboxylate transporters (MCTs) was required for induction of CES2 protein secretion. Treatment of primary hepatocytes with AR-C155858, a nanomolar dual MCT1/2 inhibitor,^{58,59} dose-dependently inhibited the lactate-induced secretion of CES2 (Figure 4F). Once again, the inhibitory effect of AR-C155858 was selective for CES2, since no changes were observed in extracellular albumin under these conditions (Figure S3H). These data demonstrate that extracellular lactate is sufficient to drive secretion of CES2 proteins via classical pathway from hepatocytes *in vitro* in a manner that requires import of lactate into hepatocytes (Figure 4G).

Secreted CES2 proteins exhibit anti-obesity, anti-diabetic, and endurance-enhancing effects in mice

We sought to determine whether release of extracellular CES2 from the liver following exercise was simply a response to exercise training, or whether soluble CES2 proteins might function as

Figure 4. Lactate-induced CES2 secretion in mouse primary hepatocytes

(A) Volcano plot of adjusted p values (–log₁₀) and exercise fold change (log₂) of albumin secretomes. Black dots indicate exercise training-regulated cell type-protein pairs (adjusted p < 0.05 and exercise fold change > 1.5) and gray dots indicate unchanged cell type-protein pairs (adjusted p > 0.05 or exercise fold change < 1.5).

(B) Anti-CES2 (bottom) blotting and quantifications of band intensity (top) of immune purified biotinylated plasma proteins from 10-week-old *Albumin*-cre male mice transduced with 3 × 10¹¹ vg AAV9-FLEX-ER-TurboID virus and exercised on a treadmill for 1 week. n = 5/group, mean ± SEM.

(C–F) Anti-CES2 blotting (bottom) and quantifications of band intensity (D–F) of conditioned medium of primary hepatocytes isolated from 8- to 12-week-old male C57BL/6J mice. Cells were treated with 2 mM indicated organic compounds (C), indicated concentrations of sodium lactate (D), sodium lactate (2 mM) and BFA (5 μg/mL) (E), and indicated concentrations of sodium lactate and AR-C155858 (F) for 4 h before analysis. CES2 band intensity was normalized to albumin signal for quantifications. Experiments in each panel contain three biological replicates, mean ± SEM.

(G) Model of CES2 secretion from cells. Exercise training-inducible rise of extracellular lactate induces release of ER-lumen-resident CES2 from hepatocytes. Functional lactate transporters and endoplasmic reticulum-Golgi vesicle transport are required for CES2 secretion.

p values for quantifications in this figure were calculated from two-tailed unpaired t tests.

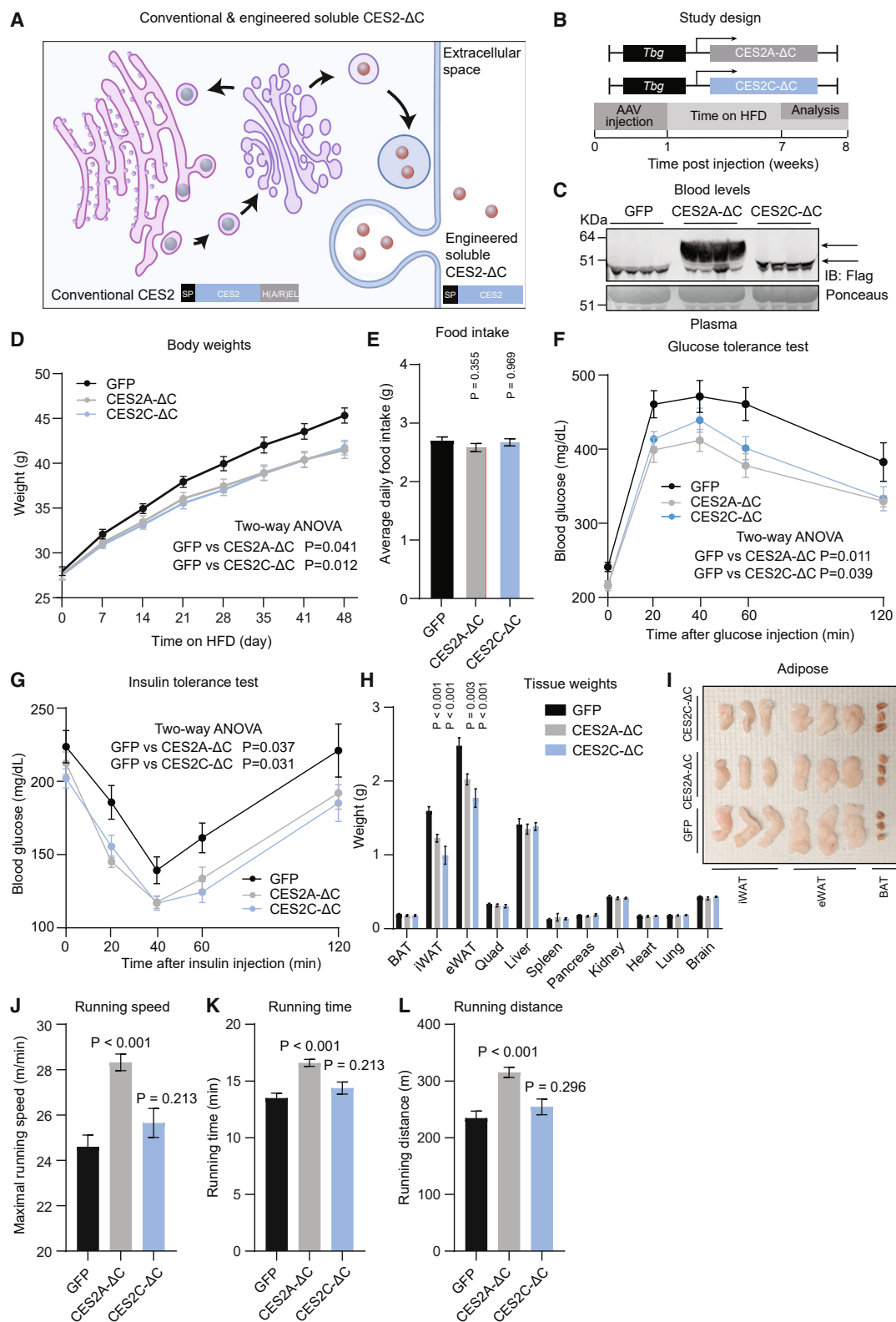


Figure 5. Secreted CES2 proteins exhibit anti-obesity, anti-diabetic, and endurance-enhancing effects in mice

(A) Cartoon schematic of conventional endoplasmic reticulum lumen localized CES2A/C (left) and engineered CES2A/C-ΔC (right). The C-terminal HXEL sequence was removed from conventional CES2A/C to generate engineered soluble CES2A/C-ΔC.

(legend continued on next page)

circulating molecular effectors of physical activity. Supporting a potential functional role for extracellular CES2, three prior studies showed that liver-specific overexpression of either human or mouse CES2 lowered body weight, reduced hepatic steatosis, and improved glucose homeostasis.^{60–62} An intestine-specific transgenic CES2C mouse model also exhibited a similarly improved metabolic phenotype.⁶³ However, these prior studies did not consider the possibility that extracellular CES2, which is likely also increased in addition to elevation of intracellular CES2 in these transgenic models, might in part mediate the anti-obesity, anti-steatosis, and anti-diabetic phenotypes observed. In addition, whether CES2 proteins might improve exercise endurance or performance had not been previously evaluated.

To directly test the functional role of extracellular CES2 in energy metabolism and glucose homeostasis without a confounding contribution from intracellular CES2, we set out to generate an engineered version of CES2 that would be exclusively localized extracellularly (Figure 5A). Analysis of the primary amino acid sequences for both murine CES2A and CES2C proteins revealed an N-terminal signal peptide, a central alpha/beta hydrolase superfamily domain with the catalytic active site GX SXG motif, and a C-terminal HXEL motif (X = A for CES2A and R for CES2C). Previous studies showed that the C-terminal HXEL motif is indispensable for the ER lumen localization and the C-terminal deleted version of CES2 can be readily detectable in the conditioned medium of cancer cells.^{64–66} We therefore generated CES2A/C constructs in which the HXEL amino acids were removed from the C terminus (CES2-ΔC) (Figure 5A). An additional N-terminal FLAG epitope tag was included after the signal peptide to aid downstream detection. Both wild-type CES2 and CES2-ΔC constructs were transfected into HEK293T cells, and the CES2 protein localization was determined by western blotting of cell lysates and conditioned media. As expected, full-length CES2A/C were enriched intracellularly, whereas both CES2A-ΔC and CES2C-ΔC proteins were exclusively found extracellularly (Figure S4A).

To deliver the engineered soluble CES2 proteins to mice, we generated an AAV (serotype 8) expressing each of our two engineered CES2A-ΔC and CES2C-ΔC constructs. CES2-ΔC was driven under the control of the hepatocyte-specific thyroxine binding protein (*Tbg*) promoter to achieve liver-specific expression (Figure 5B). Notably, we²⁸ and others^{69,70} have previously shown that the pattern of expression under the *Tbg* promoter

is largely overlapping to that of the *Albumin-cre*. Next, mice were transduced with AAV-*Tbg*-CES2A-ΔC or AAV-*Tbg*-CES2C-ΔC (n = 10/group, 10e11 GC/mouse, intravenously). Control mice were transduced with an equal titer of AAV-*Tbg*-GFP. As expected, western blotting of blood plasma using an anti-Flag antibody revealed elevation of circulating CES2A-ΔC and CES2C-ΔC (Figure 5C), which was further validated by measuring plasma ester hydrolysis activity using a previously reported synthetic substrate of carboxylesterases (Figure S4B). In contrast to blood plasma, we did not observe significant changes in total liver CES2 protein level as shown by the anti-Flag and anti-CES2 antibody staining (Figures S4C and S4D), nor an increase in liver ester hydrolysis activity (Figure S4E). These data confirm that our viral constructs increase only extracellular CES2A and CES2C levels without affecting the intracellular levels of CES2.

One week after viral transduction, mice were placed on a high-fat diet (HFD; 60% kcal from fat). Over the subsequent 7 weeks, both CES2A-ΔC and CES2C-ΔC groups of mice exhibited reduced body weight compared to mice transduced with AAV-*Tbg*-GFP (GFP 45.4 ± 0.8 g versus CES2A-ΔC 41.5 ± 0.9 g and CES2C-ΔC 41.8 ± 0.8 g, mean ± SEM) (Figure 5D). Food intake over this time period was unaltered, suggesting that the lower body weights are not simply due to reduced caloric intake (Figure 5E). In the seventh week, glucose and insulin tolerance tests revealed improved glucose clearance and insulin sensitivity in both CES2A-ΔC and CES2C-ΔC groups (Figures 5F and 5G). Dissection of tissues at the end of the experiment revealed significant reductions of inguinal white adipose tissue (iWAT) (23% and 38% reduction for CES2A-ΔC and CES2C-ΔC, respectively, versus GFP) and epididymal adipose tissue (eWAT) mass (18% and 29% reduction for CES2A-ΔC and CES2C-ΔC, respectively, versus GFP) (Figure 5H and 5I). The lean mass of all three groups remained unchanged (Figure 5H), establishing the effects on body weight are due to reduced adiposity and not any changes in lean mass. Taken together, we conclude that extracellular CES2 proteins have functions in energy balance and glucose homeostasis that are independent of their intracellular roles in triglyceride hydrolysis.

Next, we sought to understand the energy balance pathways driving the anti-obesity effects of mice overexpressing CES2A-ΔC and CES2C-ΔC. We therefore used metabolic chambers to measure parameters of whole-body energy intake and expenditure in a new cohort of virus-transduced mice. Importantly, the

(B) Cartoon schematic of the AAV constructs driven by the hepatocyte-specific *Tbg* promoter and study design of HFD feeding experiment. Eight- to 10-week-old male C57BL/6 mice were transduced with AAV-*Tbg*-CES2A-ΔC, AAV-*Tbg*-CES2C-ΔC, or AAV-*Tbg*-GFP (n = 10/group, 10e11 GC/mouse, intravenously). One week later, mice were placed on HFD feeding for 7 weeks. In the last week, glucose tolerance test and insulin tolerance test were conducted. At the end of this experiment, tissues and blood were harvested and analyzed.

(C) Anti-Flag blotting (top) or loading control (bottom) of blood plasma from 16- to 18-week-old male C57BL/6 mice injected with indicated viruses. n = 4/condition.

(D–I) Body weights over the first 7 weeks of HFD feeding (D) and food intake (measured weekly) (E), glucose tolerance test (F), insulin tolerance test (G), tissue weights (H), and inguinal white adipose tissue (iWAT), epididymal adipose tissue (eWAT), and brown adipose tissue (BAT) after 48 h of 4% PFA fixation (I) from 16- to 18-week-old male C57BL/6 mice injected with indicated viruses for 8 weeks. n = 10/condition, mean ± SEM. Samples from (I) were from randomly chosen from mice of each treatment group.

(J–L) Maximal running speed (J), total running time (K), and total running distance (L) of 16- to 18-week-old male C57BL/6 mice 8 weeks after being injected with AAV-*Tbg*-CES2A-ΔC, AAV-*Tbg*-CES2C-ΔC, or AAV-*Tbg*-GFP (n = 8–10/group, 10e11 GC/mouse, intravenously). Mice were acclimated to the treadmill 2 days prior to the maximal running tests (10 min at 10 m/min). The maximal running test was performed as previously described^{67,68} (STAR Methods). Mean ± SEM. p values for (E), (H), and (J)–(L) were calculated from two-tailed unpaired t tests. p values from (D)–(G) were calculated from two-way ANOVA with post hoc Sidak's multiple comparisons test.

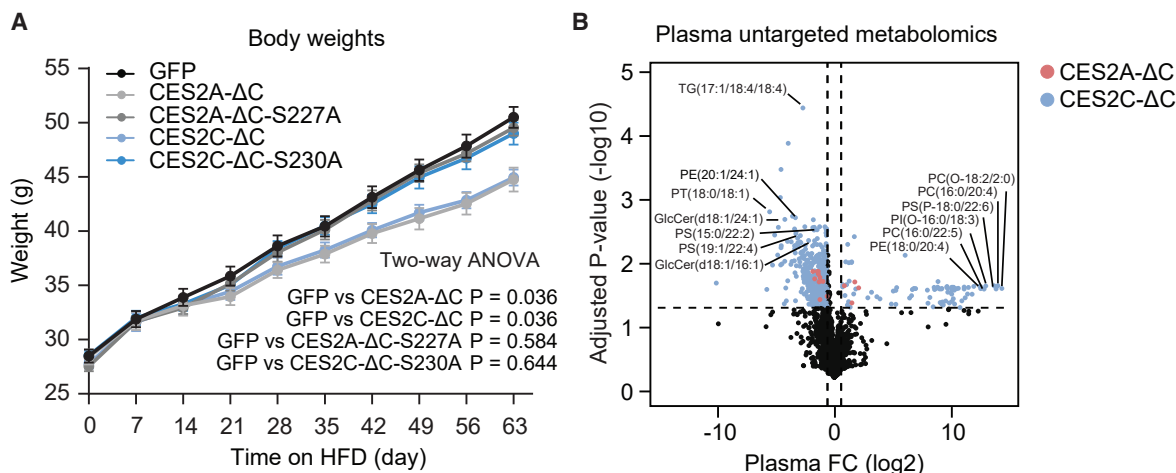


Figure 6. The anti-obesity effects of soluble CES2 proteins require enzyme activity

(A) Body weights over the first 9 weeks of HFD feeding of 18- to 20-week-old male C57BL/6 mice injected with indicated viruses ($n = 10/\text{group}$, $10e11$ GC/mouse, intravenously). Mice were fed with HFD 1 week after viral transduction. Mean \pm SEM.

(B) Untargeted metabolomic measurements of significantly changed features (adjusted $p < 0.05$ and fold change > 1.5) in blood plasma of 16- to 18-week-old male C57BL/6 mice being transduced with $10e11$ AAV-*Tbg*-CES2A- Δ C, AAV-*Tbg*-CES2C- Δ C, or AAV-*Tbg*-GFP ($n = 5/\text{group}$). Mice were placed on HFD feeding for 7 weeks before LC-MS analysis (STAR Methods).

p values for (A) were calculated from two-way ANOVA with post hoc Sidak's multiple comparisons test.

metabolic chamber measurements were performed at a time point prior to the divergence in body weights (3 weeks for CES2C- Δ C and 5 weeks for CES2A- Δ C) (Figures S4F and S4G). Both CES2A- Δ C and CES2C- Δ C overexpressing mice exhibited significantly augmented VO_2 (Figures S4H and S4I) without any effects on food intake and respiratory exchange ratio (Figures S4J–S4M). Interestingly, increased movement was observed in mice overexpressing CES2A- Δ C, but not CES2C- Δ C (Figures S4N and S4O). We conclude that the anti-obesity effects of CES2A- Δ C and CES2C- Δ C are in part due to increased whole-body energy expenditure, but via distinct physiologic mechanisms.

Quantitative mRNA analysis of limb muscles revealed broad changes in mRNA expression of genes related to cellular metabolism, fiber type, and ER Ca^{2+} handling (Figures S4P–S4R). Metabolic genes such as *Pgc1a*, *PDHa1*, *Tfam*, and *Hkll* were also robustly induced in tibialis anterior muscles of CES2A- Δ C mice (Figure S4P). We therefore next measured running speed and running endurance in CES2A- Δ C and CES2C- Δ C overexpressing animals. We transduced a new cohort of mice with AAV-*Tbg*-CES2A- Δ C, AAV-*Tbg*-CES2C- Δ C, or AAV-*Tbg*-GFP ($n = 8\text{--}10/\text{group}$, $10e11$ GC/mouse, intravenously). Over a 7-week period in which mice were fed with chow instead of HFD, body weights and food intake were unchanged (Figures S5B). Glucose and insulin tolerance tests at this time point also showed no significant differences between three groups of mice on chow diet (Figures S5C and S5D). At 8 weeks, we conducted maximal running speed tests using previously established protocols^{67,68} (STAR Methods). Mice overexpressing CES2A- Δ C, but not CES2C- Δ C, exhibited a robust 15% increase in maximal running speed, 25% increase in running time, and consequently a 34% increase in total running distance compared to GFP-transduced control mice ($p < 0.001$; Figures 5J–5L). Dissection of tissues at the end revealed consistent re-

ductions of iWAT mass (19% and 12% reduction for CES2A- Δ C and CES2C- Δ C, respectively, versus GFP) and eWAT mass (26% and 29% reduction for CES2A- Δ C and CES2C- Δ C, respectively, versus GFP). The lean mass of all three groups remained unchanged (Figure S5E). Taken together, we conclude that overexpression of CES2A- Δ C, but not CES2C- Δ C, also mimics the trained phenotype and improves running speed and endurance.

Last, to explore if the metabolic improvements from elevated soluble CES2 can be additive to exercise training's effects, we prepared a new cohort of virally transduced mice and started chronic exercise training 5 weeks on these mice 4 weeks after HFD feeding ($n = 5\text{--}6/\text{group}$, AAV-*Tbg*-GFP sedentary, AAV-*Tbg*-GFP exercise, AAV-*Tbg*-CES2A- Δ C sedentary, AAV-*Tbg*-CES2A- Δ C exercise, AAV-*Tbg*-CES2C- Δ C sedentary, and AAV-*Tbg*-CES2C- Δ C exercise) (STAR Methods). One month of chronic exercise training alone induced a very strong anti-obesity effect in all three groups of mice (sedentary versus exercise; GFP, 42.9 ± 0.9 g versus 35.8 ± 0.3 g; CES2A- Δ C, 37.3 ± 0.8 g versus 33.7 ± 1.1 g; CES2C- Δ C, 37.5 ± 0.6 g versus 32.1 ± 1.5 g) (Figures S5F–S5J). We further observed a statistically significant, additive effect of further suppression of obesity with CES2C- Δ C, but not CES2A- Δ C, overexpression (Figure S5F). Similarly, in a glucose tolerance test, exercise training in combination with CES2C- Δ C was additive, whereas exercise training in combination with CES2A- Δ C was not (Figure S5H). However, this additivity for exercise and CES2C- Δ C overexpression was not observed in the insulin tolerance test (Figure S5I). We conclude that certain metabolic benefits associated with overexpression of CES2C- Δ C, but not CES2A- Δ C, are additive with exercise training.

Are the enzymatic activities required for any of the physiologic functions of soluble CES2 proteins? To answer this question, we generated enzymatically dead versions of wild-type CES2- Δ C

(CES2A- Δ C-S227A and CES2C- Δ C-S230A, respectively). We validated complete loss of enzymatic activities of these mutant proteins using activity assays measuring hydrolysis of the prototypical artificial substrate 4-nitrophenyl acetate (Figure S6A). Next, we cloned these two genes into AAV-*Tbg* vectors and transduced a new cohort of mice ($n = 10/\text{group}$, AAV-*Tbg*-CES2A- Δ C, AAV-*Tbg*-CES2A- Δ C-S227A, AAV-*Tbg*-CES2C- Δ C, AAV-*Tbg*-CES2C- Δ C-S230A, or AAV-*Tbg*-GFP, 10×10^6 GC/mouse, intravenously). Western blotting of blood plasma using an anti-Flag antibody revealed a similar expression level between wild-type and mutant CES2A- Δ C and CES2C- Δ C, respectively (Figure S6B), demonstrating unchanged protein secretion and stability of wild-type and mutant proteins in blood plasma. One week after viral transduction, mice were placed on HFD (60% kcal from fat). Over the subsequent 9 weeks, as expected both CES2A- Δ C and CES2C- Δ C groups of mice exhibited reduced body weight compared to mice transduced with AAV-*Tbg*-GFP (GFP 50.5 ± 1.0 g versus CES2A- Δ C 44.8 ± 1.1 g and CES2C- Δ C 45.0 ± 0.7 g, mean \pm SEM). The catalytic activity of the soluble CES2 proteins was required for this effect since both mutant groups exhibited identical body weight to control HFD-fed mice (CES2A- Δ C-S227A 49.5 ± 0.7 g and CES2C- Δ C-S230A 49.0 ± 1.0 g, mean \pm SEM) (Figure 6A). Food intake was not changed among all groups of mice (Figure S6C).

To understand potential substrates of soluble CES2 proteins that might be downstream effectors of their anti-obesity effects, we performed untargeted metabolomics on plasma from CES2A- Δ C, CES2C- Δ C, or GFP-transduced mice (STAR Methods). Differential peaks were identified by XCMS, and lipid structural assignments were made using the METLIN database.⁷¹ A total of 462 metabolite features were changed by elevated soluble CES2C (43.6% of total detected features, adjusted $p < 0.05$, FC > 1.5 , versus GFP) whereas soluble CES2A exhibited modest effects on 15 features (1.6% of total detected features, adjusted $p < 0.05$, FC > 1.5 , versus GFP) (Figure 6B; Table S4). Interestingly, $\sim 30\%$ of changed metabolite features were annotated as lipids, such as phosphatidylserine (PS), phosphatidylethanolamine (PE), phosphoinositide (PI), phosphatidylcholine (PC), ceramide, and acylglycerol (Figure 6B). These data suggest that soluble CES2C- Δ C induces profound alterations in the circulating lipid species that correlate with its anti-obesity effects, whereas the anti-obesity effects of CES2A- Δ C are not correlated with as widespread dysregulation of plasma lipid species. These data further provide evidence that CES2A- Δ C and CES2C- Δ C exert their anti-obesity effects via distinct mechanistic pathways.

DISCUSSION

Here we have generated an organism-wide proteomic dataset of the cell-type-specific secretome responses to 1 week of treadmill running. In contrast to previous efforts that have focused on individual secreted factors or individual cell types, our current dataset provides several insights of potential importance to our understanding of cell and tissue crosstalk during physical activity, including (1) the demonstration that $\sim 20\%$ of cell type-protein pairs exhibit complex, bidirectional, and cell-type-specific regulation following exercise training; (2) the identification of *Pdgfra* cells as a highly responsive cell type to exercise training;

(3) evidence that the production of non-canonical secreted proteoforms contributes to exercise training-regulated tissue crosstalk; and (4) discovery of secreted CES2 as extracellular enzymes with anti-obesity, anti-diabetic, and endurance-enhancing functions.

Classically, muscle has been studied as a principal source of activity-inducible “myokines” that mediate tissue crosstalk in exercise training. More recent evidence has expanded this model to include exercise training-inducible hepatokines from the liver⁷² and adipokines from the fat.²³ In general, many of these past studies have focused on individual cell types. Our studies suggest that many more cell types respond to exercise training than previously recognized, including *Pdgfra*⁺ cells distributed to multiple organ systems. Recent reports using single-cell RNA sequencing showed that exercise training regulation in adipose was most strongly pronounced in adipose stem cells,⁷³ which are defined by the expression of *Pdgfra*.⁷⁴ These adipose-resident fibroblasts may indeed correspond to a subset of the *Pdgfra*⁺ cells identified in our secretome profiling dataset. In the future, it will be important to specifically determine which exercise training-regulated cell types and which organs beyond adipose are defined by *Pdgfra*⁺ expression.

Forty percent of multi-origin secreted proteins detected in our study exhibit bidirectional change after exercise training, meaning that their secretion is upregulated in certain cell types following exercise training and downregulated in others. The cell-type-specific nature of this regulation underscores the importance of cell-type-specific resolution for the analysis of complex perturbations, rather than bulk measurements from total plasma. Currently, why the same protein can have different directionality after exercise training in different cell types remains unknown. We speculate that one possibility is due to cell-type-specific differences in the response to exercise training-regulated hormones, which may functionally result in different intracellular regulation of the secretory pathway in a cell-type-dependent manner. Mechanistic dissection of these differences could provide important clues to the cell-type-specific responses of exercise training.

Several lines of evidence suggest that the cell-type-specific changes found in our dataset indeed reflect bulk changes to circulating protein levels. For instance, we can find specific examples of exercise training-inducible proteins that have been reported in the literature by bulk plasma measurements, and that are also changed in our dataset (e.g., TIMP3,⁷⁵ SOD3^{47–50}). Nevertheless, future studies to understand the correlation of biotinylated protein levels with total plasma protein levels at a global scale will only be enabled by higher sensitivity, targeted shotgun proteomics, or aptamer-based arrays that can be used for mouse plasma proteins.

Using cell culture systems, we also provide evidence that the exercise training-inducible secretion of CES2 from the liver can be recapitulated by addition of extracellular lactate to primary hepatocytes *in vitro*. While the precise downstream mechanism linking lactate import to protein secretion from hepatocytes remains unknown, we suspect one likely possibility includes lactate-inducible proteolytic cleavage of the CES2 C terminus. This C terminus contains the endoplasmic reticulum retention signal required for intracellular localization of CES2. In addition, RHBDL4 has been proposed as a hydrolase that liberates an

array of endoplasmic reticulum-resident proteins into the extracellular space.⁷⁶ Consistent with this idea, we were unable to detect peptides corresponding to the C terminus of either CES2A or CES2C (Figure S6D). Such an endoplasmic reticulum-retention signal cleavage mechanism may also explain the secretion of several other endoplasmic reticulum-resident proteins in our dataset, such as H6PD (in *Adiponectin*-cre secretomes), CALX (in *Albumin*-cre and *Lysm*-cre secretomes), and AT2A1 (in *MCK*-cre secretomes). The possibility that lactate itself constitutes a more general mechanism linking physical activity to secreted protein-mediated tissue crosstalk remains an open question for future work.

We also provide evidence that exercise training-inducible secretion of CES2 proteins is not simply a molecular response to exercise training. Instead, using engineered versions of CES2 that are localized exclusively extracellularly, we show that soluble CES2 proteins exhibit anti-obesity, anti-diabetic, and performance-enhancing actions in mice. The anti-obesity and anti-diabetic observations here further refine the interpretation of previous CES2 transgenic models: whereas those previous mouse models likely induced both intracellular and extracellular CES2 proteins, our exclusively extracellular CES2A- Δ C and CES2C- Δ C constructs demonstrate that circulating CES2 proteins are sufficient to reproduce at least some of the metabolically beneficial phenotypes. In addition, the ability for CES2A- Δ C, but not CES2C- Δ C, to enhance running speed and endurance was a novel finding. Last, the *CES2* locus has been linked to multiple cardiometabolic parameters in the UK Biobank, including HDL cholesterol ($p = 5.14e-311$, $\beta = +0.0625$), blood pressure ($p = 1.64e-17$, $\beta = +0.0317$), and BMI-adjusted waist-hip ratio ($p = 4.61e-15$, $\beta = -0.0297$), suggesting that exercise training-regulated soluble CES2 proteins might also impact cardiometabolic health in humans.

The variation of detectable *TurboID* mRNA across different tissues suggests varying secretome labeling efficiencies among cell types. Several reasons likely contribute to this variation, including differential AAV transduction efficiency between cell types, as well as the isolation of total organ mRNA when potentially only a small number of particular target cell types are transduced. Notably, we are only comparing the effect of exercise training within the same Cre transduced line (e.g., each Cre serves as its own control) and therefore avoid the confounding factor of varying *TurboID* expression. Transgenic *TurboID* mice will be a valuable resource in future work to standardize and increase labeling efficiency, especially in non-transducible cell types.

Projecting forward, an important extension of this work will be to understand the effects of different exercise training regimes and training time on the cellular secretomes *in vivo*. Which of the secretome responses observed here are specific to the training protocol used in this study, and which might be general responses to multiple types of exercise training? Our time course of *Pdgfra*-cre secretomes in response to exercise training already provides evidence that the secretome responses can be complex and time dependent. Indeed, a single bout versus multiple bouts of either aerobic or resistance training produces distinct phenotypic responses that correlate with activation of overlapping yet distinct molecular pathways.^{77,78} On the other hand, our identification of a functional coupling between lactate and CES2 secretion from the liver suggests that soluble CES2 may be a molecular

effector more generally associated with multiple and distinct modalities of physical activity. In addition, these murine datasets will need to be compared with studies of exercise plasma in large and deeply phenotyped human cohorts^{79,80} to determine which molecular changes might be conserved or species specific. Ultimately, we anticipate that these and other organism-wide datasets will provide a systematic foundation for probing the role of secreted proteins as mediators of tissue crosstalk in exercise training and as molecular effectors of physical activity across the diverse cell and organs systems across the body.

Limitations of study

We acknowledge several limitations of this study. First, there may be other mechanisms regulating a secreted protein's circulating levels beyond secretion alone, including proteolytic degradation and/or other clearance mechanisms. Consequently, our dataset may also contain false negatives (e.g., bona fide exercise training-inducible proteins) because of these additional regulatory mechanisms for circulating proteins. Second, our secretome dataset does not distinguish between which molecular changes are acute versus adaptive. Third, the use of a 1-week treadmill running perturbation in this study leads to the activation of exercise training markers in the skeletal muscle, as well as a slight reduction in body weight, fat mass, and food intake in mice. Although these phenotypes are commonly associated with exercise training, it is not possible to determine the individual contribution of each factor to the changes detected in the secretome. Fourth, our studies have not performed any loss-of-function studies that selectively ablate extracellular, but not intracellular, CES2 functions. The discovery and development of neutralizing CES2 antibodies would enable these important studies. Fifth, there remains a possibility for sex-specific secretome effects in cell types beyond *Pdgfra*+ cells, which would be an area of potentially interesting future study. Finally, our treadmill running was performed in the morning, corresponding to the early rest phase in mice. Although this experimental condition may potentially activate a circadian rhythm-dependent secretome response, the detected changes in the secretome are likely attributable to the exercise training itself, as both the sedentary control and exercise training animals were similarly perturbed. Additionally, no changes in individual proteins derived from hepatocytes, such as CES2, were observed due to the disruption of circadian rhythm (data not shown). On the other hand, growing evidence suggests interplay and crosstalk between exercise training and circadian rhythms.^{22,81-83} Our secretome profiling approach may be useful for providing high-resolution profiling in future studies that seek to dissect the relationship between exercise and circadian rhythms.

STAR★METHODS

Detailed methods are provided in the online version of this paper and include the following:

- KEY RESOURCES TABLE
- RESOURCE AVAILABILITY
 - Lead contact
 - Materials availability
 - Data and code availability

- **EXPERIMENTAL MODEL AND SUBJECT DETAILS**
 - Mouse models
- **METHOD DETAILS**
 - Cell line cultures
 - Western blotting
 - AAV production
 - Viral transduction
 - Mouse exercise and secretome labeling protocols
 - Quantitative PCR
 - Plasma and tissue sample preparation from mice
 - Proteomic sample processing
 - Proteomics data acquisition
 - Proteomics data analysis to generate cell type-protein pairs
 - Exercise responsiveness scores calculations
 - Time course of *Pdgfra*-cre secretomes
 - Gene ontology analysis
 - Isolation and culture of primary mouse hepatocytes
 - Treatment of hepatocytes with organic compounds, MCT inhibitor and brefeldin A
 - Construction of plasmids for overexpression of CES2A/C-ΔC
 - Generation of recombinant CES2 proteins
 - Determination of CES2A-ΔC and CES2C-ΔC secretion in cell culture
 - Histology
 - Glucose tolerance and insulin tolerance tests in mice
 - Maximal running capacity test
 - Chronic treadmill running
 - Indirect calorimetry and physiological measurements
 - LC-MS detection of blood plasma lactate
 - Untargeted metabolomics by LC-MS
 - Carboxylesterases enzymatic activity measurement
- **QUANTIFICATION AND STATISTICAL ANALYSIS**
 - Data representation and statistical analysis

SUPPLEMENTAL INFORMATION

Supplemental information can be found online at <https://doi.org/10.1016/j.cmet.2023.04.011>.

ACKNOWLEDGMENTS

We thank members of the Long, Bertozzi, and Svensson labs for helpful discussions. We gratefully acknowledge the staff at the Penn Vector Core (RRID: SCR_022432) for the production of AAVs. This work was supported by the US National Institutes of Health (DK105203 and DK124265 to J.Z.L., DK125260 and DK111916 to K.J.S., and K99GM147304 to N.M.R.), the Wu Tsai Human Performance Alliance (research grant to J.Z.L. and postdoctoral fellowship to X.L.), the Stanford Diabetes Research Center (P30DK116074), the Stanford Cardiovascular Institute (CVI), the Weintz Family COVID-19 research fund (K.J.S.), the American Heart Association (AHA), the Stanford School of Medicine, the Jacob Churg Foundation (K.J.S.), the McCormick and Gabilan Award (K.J.S.), the Vanessa Kong-Kerzner Foundation (graduate fellowship to W.W.), the American Heart Association (postdoctoral fellowship to M.Z.), Fundacion Alfonso Martin Escudero (postdoctoral fellowship to M.D.M.-G.), Independent Research Fund Denmark (2030-00007A), and the Lundbeck Foundation (R380-2021-1451) (S.H.R.).

AUTHOR CONTRIBUTIONS

Conceptualization, W.W., N.M.R., and J.Z.L.; methodology, W.W., N.M.R., and X.L.; investigation, W.W., N.M.R., X.L., X.S., S.H.R., J.G., M.Z.,

M.D.M.-G., H.B., A.S.-H.T., V.L.L., W.H., and A.L.W.; writing – original draft, W.W., N.M.R., and J.Z.L.; writing – review & editing, W.W., N.M.R., X.L., and J.Z.L.; resources, J.Z.L., C.R.B., K.J.S., and M.P.S.; supervision and funding acquisition, J.Z.L. and C.R.B.

DECLARATION OF INTERESTS

Stanford University has filed a provisional patent on extracellular CES2 proteins and methods of use.

Received: September 14, 2022

Revised: February 21, 2023

Accepted: April 5, 2023

Published: May 3, 2023

REFERENCES

1. Piercy, K.L., Troiano, R.P., Ballard, R.M., Carlson, S.A., Fulton, J.E., Galuska, D.A., George, S.M., and Olson, R.D. (2018). The physical activity guidelines for Americans. *JAMA* 320, 2020–2028. <https://doi.org/10.1001/jama.2018.14854>.
2. Warburton, D.E.R., and Bredin, S.S.D. (2017). Health benefits of physical activity: a systematic review of current systematic reviews. *Curr. Opin. Cardiol.* 32, 541–556. <https://doi.org/10.1097/HCO.0000000000000437>.
3. Lear, S.A., Hu, W., Rangarajan, S., Gasevic, D., Leong, D., Iqbal, R., Casanova, A., Swaminathan, S., Anjana, R.M., Kumar, R., et al. (2017). The effect of physical activity on mortality and cardiovascular disease in 130 000 people from 17 high-income, middle-income, and low-income countries: the PURE study. *Lancet* 390, 2643–2654. [https://doi.org/10.1016/S0140-6736\(17\)31634-3](https://doi.org/10.1016/S0140-6736(17)31634-3).
4. Booth, F.W., Roberts, C.K., Thyfault, J.P., Rueggsegger, G.N., and Toedebusch, R.G. (2017). Role of inactivity in chronic diseases: evolutionary insight and pathophysiological mechanisms. *Physiol. Rev.* 97, 1351–1402. <https://doi.org/10.1152/physrev.00019.2016>.
5. Knowler, W.C., Barrett-Connor, E., Fowler, S.E., Hamman, R.F., Lachin, J.M., Walker, E.A., and Nathan, D.M.; Diabetes Prevention Program Research Group (2002). Reduction in the incidence of type 2 diabetes with lifestyle intervention or metformin. *N. Engl. J. Med.* 346, 393–403. <https://doi.org/10.1056/NEJMoa012512>.
6. Hambrecht, R., Walther, C., Möbius-Winkler, S., Gielen, S., Linke, A., Conradi, K., Erbs, S., Kluge, R., Kendziorra, K., Sabri, O., et al. (2004). Percutaneous coronary angioplasty compared with exercise training in patients with stable coronary artery disease: a randomized trial. *Circulation* 109, 1371–1378. <https://doi.org/10.1161/01.CIR.0000121360.31954>.
7. Blair, S.N., Kohl, H.W., 3rd, Paffenbarger, R.S., Jr., Clark, D.G., Cooper, K.H., and Gibbons, L.W. (1989). Physical fitness and all-cause mortality. A prospective study of healthy men and women. *JAMA* 262, 2395–2401. <https://doi.org/10.1001/jama.262.17.2395>.
8. Neuffer, P.D., Bamman, M.M., Muoio, D.M., Bouchard, C., Cooper, D.M., Goodpaster, B.H., Booth, F.W., Kohrt, W.M., Gerszten, R.E., Mattson, M.P., et al. (2015). Understanding the cellular and molecular mechanisms of physical activity-induced health benefits. *Cell Metab.* 22, 4–11. <https://doi.org/10.1016/j.cmet.2015.05.011>.
9. McGee, S.L., and Hargreaves, M. (2020). Exercise adaptations: molecular mechanisms and potential targets for therapeutic benefit. *Nat. Rev. Endocrinol.* 16, 495–505. <https://doi.org/10.1038/s41574-020-0377-1>.
10. Chow, L.S., Gerszten, R.E., Taylor, J.M., Pedersen, B.K., van Praag, H., Trappe, S., Febbraio, M.A., Galis, Z.S., Gao, Y., Haus, J.M., et al. (2022). Exerkines in health, resilience and disease. *Nat. Rev. Endocrinol.* 18, 273–289. <https://doi.org/10.1038/s41574-022-00641-2>.
11. Safdar, A., Saleem, A., and Tarnopolsky, M.A. (2016). The potential of endurance exercise-derived exosomes to treat metabolic diseases. *Nat. Rev. Endocrinol.* 12, 504–517. <https://doi.org/10.1038/nrendo.2016.76>.

12. Goldstein, M.S. (1961). Humoral nature of the hypoglycemic factor of muscular work. *Diabetes* 10, 232–234. <https://doi.org/10.2337/diab.10.3.232>.
13. Horowitz, A.M., Fan, X., Bieri, G., Smith, L.K., Sanchez-Diaz, C.I., Schroer, A.B., Gontier, G., Casaletto, K.B., Kramer, J.H., Williams, K.E., and Villeda, S.A. (2020). Blood factors transfer beneficial effects of exercise on neurogenesis and cognition to the aged brain. *Science* 369, 167–173. <https://doi.org/10.1126/science.aaw2622>.
14. De Miguel, Z., Khoury, N., Betley, M.J., Lehallier, B., Willoughby, D., Olsson, N., Yang, A.C., Hahn, O., Lu, N., Vest, R.T., et al. (2021). Exercise plasma boosts memory and dampens brain inflammation via clusterin. *Nature* 600, 494–499. <https://doi.org/10.1038/s41586-021-04183-x>.
15. Steensberg, A., van Hall, G., Osada, T., Sacchetti, M., Saltin, B., and Klarlund Pedersen, B. (2000). Production of interleukin-6 in contracting human skeletal muscles can account for the exercise-induced increase in plasma interleukin-6. *J. Physiol.* 529, 237–242. <https://doi.org/10.1111/j.1469-7793.2000.00237.x>.
16. Knudsen, N.H., Stanya, K.J., Hyde, A.L., Chalom, M.M., Alexander, R.K., Liou, Y.H., Starost, K.A., Gangl, M.R., Jacobi, D., Liu, S., et al. (2020). Interleukin-13 drives metabolic conditioning of muscle to endurance exercise. *Science* 368, eaat3987. <https://doi.org/10.1126/science.aat3987>.
17. Boström, P., Wu, J., Jedrychowski, M.P., Korde, A., Ye, L., Lo, J.C., Rasbach, K.A., Bostrom, E.A., Choi, J.H., Long, J.Z., et al. (2012). A PGC1- α -dependent myokine that drives brown-fat-like development of white fat and thermogenesis. *Nature* 481, 463–468. <https://doi.org/10.1038/nature10777>.
18. Wrann, C.D., White, J.P., Salogiannis, J., Laznik-Bogoslavski, D., Wu, J., Ma, D., Lin, J.D., Greenberg, M.E., and Spiegelman, B.M. (2013). Exercise induces hippocampal BDNF through a PGC-1 α /FNDC5 pathway. *Cell Metab.* 18, 649–659. <https://doi.org/10.1016/j.cmet.2013.09.008>.
19. Rao, R.R., Long, J.Z., White, J.P., Svensson, K.J., Lou, J., Lokurkar, I., Jedrychowski, M.P., Ruas, J.L., Wrann, C.D., Lo, J.C., et al. (2014). Meteorin-like is a hormone that regulates immune-adipose interactions to increase beige fat thermogenesis. *Cell* 157, 1279–1291. <https://doi.org/10.1016/j.cell.2014.03.065>.
20. Reddy, A., Bozi, L.H.M., Yaghi, O.K., Mills, E.L., Xiao, H., Nicholson, H.E., Paschini, M., Paulo, J.A., Garrity, R., Laznik-Bogoslavski, D., et al. (2020). pH-gated succinate secretion regulates muscle remodeling in response to exercise. *Cell* 183, 62–75.e17. <https://doi.org/10.1016/j.cell.2020.08.039>.
21. Agudelo, L.Z., Femenia, T., Orhan, F., Porsmyr-Palmertz, M., Goiny, M., Martinez-Redondo, V., Correia, J.C., Izadi, M., Bhat, M., Schuppe-Koistinen, I., et al. (2014). Skeletal muscle PGC-1 α 1 modulates kynurenine metabolism and mediates resilience to stress-induced depression. *Cell* 159, 33–45. <https://doi.org/10.1016/j.cell.2014.07.051>.
22. Sato, S., Dyar, K.A., Treebak, J.T., Jepsen, S.L., Ehrlich, A.M., Ashcroft, S.P., Trost, K., Kunzke, T., Prade, V.M., Small, L., et al. (2022). Atlas of exercise metabolism reveals time-dependent signatures of metabolic homeostasis. *Cell Metab.* 34, 329–345.e8. <https://doi.org/10.1016/j.cmet.2021.12.016>.
23. Takahashi, H., Alves, C.R.R., Stanford, K.I., Middelbeek, R.J.W., Nigro, P., Ryan, R.E., Xue, R., Sakaguchi, M., Lynes, M.D., So, K., et al. (2019). TGF- β 2 is an exercise-induced adipokine that regulates glucose and fatty acid metabolism. *Nat. Metab.* 1, 291–303. <https://doi.org/10.1038/s42255-018-0030-7>.
24. Lynes, M.D., Leiria, L.O., Lundh, M., Bartelt, A., Shamsi, F., Huang, T.L., Takahashi, H., Hirshman, M.F., Schlein, C., Lee, A., et al. (2017). The cold-induced lipokine 12,13-diHOME promotes fatty acid transport into brown adipose tissue. *Nat. Med.* 23, 631–637. <https://doi.org/10.1038/nm.4297>.
25. Uhlén, M., Fagerberg, L., Hallström, B.M., Lindskog, C., Oksvold, P., Mardinoglu, A., Sivertsson, A., Kampf, C., Sjostedt, E., Asplund, A., et al. (2015). Proteomics. Tissue-based map of the human proteome. *Science* 347, 1260419. <https://doi.org/10.1126/science.1260419>.
26. Somninen, H.K., Boivin, G.P., and Elased, K.M. (2014). Daily exercise training protects against albuminuria and angiotensin converting enzyme 2 shedding in db/db diabetic mice. *J. Endocrinol.* 221, 235–251. <https://doi.org/10.1530/JOE-13-0532>.
27. Wei, W., Riley, N.M., Lyu, X., Bertozzi, C.R., and Long, J.Z. (2021). Protocol for cell type-specific labeling, enrichment, and proteomic profiling of plasma proteins in mice. *STAR Protoc.* 2, 101014. <https://doi.org/10.1016/j.xpro.2021.101014>.
28. Wei, W., Riley, N.M., Yang, A.C., Kim, J.T., Terrell, S.M., Li, V.L., Garcia-Contreras, M., Bertozzi, C.R., and Long, J.Z. (2021). Cell type-selective secretome profiling in vivo. *Nat. Chem. Biol.* 17, 326–334. <https://doi.org/10.1038/s41589-020-00698-y>.
29. Droujinine, I.A., Meyer, A.S., Wang, D., Udeshi, N.D., Hu, Y., Rocco, D., McMahon, J.A., Yang, R., Guo, J., Mu, L., et al. (2021). Proteomics of protein trafficking by in vivo tissue-specific labeling. *Nat. Commun.* 12, 2382. <https://doi.org/10.1038/s41467-021-22599-x>.
30. Kim, K.E., Park, I., Kim, J., Kang, M.G., Choi, W.G., Shin, H., Kim, J.S., Rhee, H.W., and Suh, J.M. (2021). Dynamic tracking and identification of tissue-specific secretory proteins in the circulation of live mice. *Nat. Commun.* 12, 5204. <https://doi.org/10.1038/s41467-021-25546-y>.
31. Liu, J., Jang, J.Y., Pirooznia, M., Liu, S., and Finkel, T. (2021). The secretome mouse provides a genetic platform to delineate tissue-specific in vivo secretion. *Proc. Natl. Acad. Sci. USA* 118, e2005134118. <https://doi.org/10.1073/pnas.2005134118>.
32. Branon, T.C., Bosch, J.A., Sanchez, A.D., Udeshi, N.D., Svinkina, T., Carr, S.A., Feldman, J.L., Perrimon, N., and Ting, A.Y. (2018). Efficient proximity labeling in living cells and organisms with TurboID. *Nat. Biotechnol.* 36, 880–887. <https://doi.org/10.1038/nbt.4201>.
33. Zicarelli, C., Soltys, S., Rengo, G., and Rabinowitz, J.E. (2008). Analysis of AAV serotypes 1–9 mediated gene expression and tropism in mice after systemic injection. *Mol. Ther.* 16, 1073–1080. <https://doi.org/10.1038/mt.2008.76>.
34. Wu, J., Ruas, J.L., Estall, J.L., Rasbach, K.A., Choi, J.H., Ye, L., Bostrom, P., Tyra, H.M., Crawford, R.W., Campbell, K.P., et al. (2011). The unfolded protein response mediates adaptation to exercise in skeletal muscle through a PGC-1 α /ATF6 α complex. *Cell Metab.* 13, 160–169. <https://doi.org/10.1016/j.cmet.2011.01.003>.
35. Finck, B.N., and Kelly, D.P. (2006). PGC-1 coactivators: inducible regulators of energy metabolism in health and disease. *J. Clin. Invest.* 116, 615–622. <https://doi.org/10.1172/JCI27794>.
36. Kawasaki, E., Hokari, F., Sasaki, M., Sakai, A., Koshinaka, K., and Kawanaka, K. (2009). Role of local muscle contractile activity in the exercise-induced increase in NR4A receptor mRNA expression. *J. Appl. Physiol.* 106, 1826–1831. <https://doi.org/10.1152/jappphysiol.90923.2008>.
37. Lewis, G.D., Farrell, L., Wood, M.J., Martinovic, M., Arany, Z., Rowe, G.C., Souza, A., Cheng, S., McCabe, E.L., Yang, E., et al. (2010). Metabolic signatures of exercise in human plasma. *Sci. Transl. Med.* 2, 33ra37. <https://doi.org/10.1126/scitranslmed.3001006>.
38. Searle, B.C., Pino, L.K., Egerton, J.D., Ting, Y.S., Lawrence, R.T., MacLean, B.X., Villen, J., and MacCoss, M.J. (2018). Chromatogram libraries improve peptide detection and quantification by data independent acquisition mass spectrometry. *Nat. Commun.* 9, 5128. <https://doi.org/10.1038/s41467-018-07454-w>.
39. Pino, L.K., Just, S.C., MacCoss, M.J., and Searle, B.C. (2020). Acquiring and analyzing data independent acquisition proteomics experiments without spectrum libraries. *Mol. Cell. Proteomics* 19, 1088–1103. <https://doi.org/10.1074/mcp.P119.001913>.
40. Tyanova, S., Temu, T., Sinitcyn, P., Carlson, A., Hein, M.Y., Geiger, T., Mann, M., and Cox, J. (2016). The Perseus computational platform for comprehensive analysis of (pro)teomics data. *Nat. Methods* 13, 731–740. <https://doi.org/10.1038/nmeth.3901>.

41. Pino, L.K., Searle, B.C., Bollinger, J.G., Nunn, B., MacLean, B., and MacCoss, M.J. (2020). The Skyline ecosystem: informatics for quantitative mass spectrometry proteomics. *Mass Spectrom. Rev.* **39**, 229–244. <https://doi.org/10.1002/mas.21540>.
42. Stern, J.H., Rutkowski, J.M., and Scherer, P.E. (2016). Adiponectin, leptin, and fatty acids in the maintenance of metabolic homeostasis through adipose tissue crosstalk. *Cell Metab.* **23**, 770–784. <https://doi.org/10.1016/j.cmet.2016.04.011>.
43. Liu, H., Chen, S.E., Jin, B., Carson, J.A., Niu, A., Durham, W., Lai, J.Y., and Li, Y.P. (2010). TIMP3: a physiological regulator of adult myogenesis. *J. Cell Sci.* **123**, 2914–2921. <https://doi.org/10.1242/jcs.057620>.
44. Hanaoka, Y., Yasuda, O., Soejima, H., Miyata, K., Yamamoto, E., Izumiya, Y., Maeda, N., Ohishi, M., Rakugi, H., Oike, Y., et al. (2014). Tissue inhibitor of metalloproteinase-3 knockout mice exhibit enhanced energy expenditure through thermogenesis. *PLoS One* **9**, e94930. <https://doi.org/10.1371/journal.pone.0094930>.
45. Basu, R., Lee, J., Morton, J.S., Takawale, A., Fan, D., Kandalam, V., Wang, X., Davidge, S.T., and Kassiri, Z. (2013). TIMP3 is the primary TIMP to regulate agonist-induced vascular remodelling and hypertension. *Cardiovasc. Res.* **98**, 360–371. <https://doi.org/10.1093/cvr/cvt067>.
46. Stöhr, R., Cavallera, M., Menini, S., Mavilio, M., Casagrande, V., Rossi, C., Urbani, A., Cardellini, M., Pugliese, G., Menghini, R., and Federici, M. (2014). Loss of TIMP3 exacerbates atherosclerosis in ApoE null mice. *Atherosclerosis* **235**, 438–443. <https://doi.org/10.1016/j.atherosclerosis.2014.05.946>.
47. Abdelsaid, K., Sudhakar, V., Harris, R.A., Das, A., Youn, S.W., Liu, Y., McMenamin, M., Hou, Y., Fulton, D., Hamrick, M.W., et al. (2022). Exercise improves angiogenic function of circulating exosomes in type 2 diabetes: role of exosomal SOD3. *FASEB J* **36**, e22177. <https://doi.org/10.1096/fj.202101323R>.
48. Hitomi, Y., Watanabe, S., Kizaki, T., Sakurai, T., Takemasa, T., Haga, S., Ookawara, T., Suzuki, K., and Ohno, H. (2008). Acute exercise increases expression of extracellular superoxide dismutase in skeletal muscle and the aorta. *Redox Rep.* **13**, 213–216. <https://doi.org/10.1179/135100008X308894>.
49. Fukai, T., Siegfried, M.R., Ushio-Fukai, M., Cheng, Y., Kojda, G., and Harrison, D.G. (2000). Regulation of the vascular extracellular superoxide dismutase by nitric oxide and exercise training. *J. Clin. Invest.* **105**, 1631–1639. <https://doi.org/10.1172/JCI9551>.
50. Kusuyama, J., Alves-Wagner, A.B., Conlin, R.H., Makarewicz, N.S., Albertson, B.G., Prince, N.B., Kobayashi, S., Kozuka, C., Moller, M., Bjerre, M., et al. (2021). Placental superoxide dismutase 3 mediates benefits of maternal exercise on offspring health. *Cell Metab.* **33**, 939–956.e8. <https://doi.org/10.1016/j.cmet.2021.03.004>.
51. Raschke, S., Eckardt, K., Bjorklund Holven, K., Jensen, J., and Eckel, J. (2013). Identification and validation of novel contraction-regulated myokines released from primary human skeletal muscle cells. *PLoS One* **8**, e62008. <https://doi.org/10.1371/journal.pone.0062008>.
52. Duggan, C., Xiao, L., Wang, C.Y., and McTiernan, A. (2014). Effect of a 12-month exercise intervention on serum biomarkers of angiogenesis in postmenopausal women: a randomized controlled trial. *Cancer Epidemiol. Biomarkers Prev.* **23**, 648–657. <https://doi.org/10.1158/1055-9965.EPI-13-1155>.
53. Zepp, J.A., Zacharias, W.J., Frank, D.B., Cavanaugh, C.A., Zhou, S., Morley, M.P., and Morrissey, E.E. (2017). Distinct mesenchymal lineages and niches promote epithelial self-renewal and myofibrogenesis in the lung. *Cell* **170**, 1134–1148.e10. <https://doi.org/10.1016/j.cell.2017.07.034>.
54. Li, R., Bernau, K., Sandbo, N., Gu, J., Preissl, S., and Sun, X. (2018). Pdgfra marks a cellular lineage with distinct contributions to myofibroblasts in lung maturation and injury response. *eLife* **7**, e36865. <https://doi.org/10.7554/eLife.36865>.
55. Merrick, D., Sakers, A., Irgebay, Z., Okada, C., Calvert, C., Morley, M.P., Percec, I., and Seale, P. (2019). Identification of a mesenchymal progenitor cell hierarchy in adipose tissue. *Science* **364**, eaav2501. <https://doi.org/10.1126/science.aav2501>.
56. Schraner, D., Kastenmuller, G., Schonfelder, M., Romisch-Margl, W., and Wackerhage, H. (2020). Metabolite concentration changes in humans after a bout of exercise: a systematic review of exercise metabolomics studies. *Sports Med. Open* **6**, 11. <https://doi.org/10.1186/s40798-020-0238-4>.
57. Contrepois, K., Wu, S., Moneghetti, K.J., Hornburg, D., Ahadi, S., Tsai, M.S., Metwally, A.A., Wei, E., Lee-McMullen, B., Quijada, J.V., et al. (2020). Molecular choreography of acute exercise. *Cell* **181**, 1112–1130.e16. <https://doi.org/10.1016/j.cell.2020.04.043>.
58. Ovens, M.J., Davies, A.J., Wilson, M.C., Murray, C.M., and Halestrap, A.P. (2010). AR-C155858 is a potent inhibitor of monocarboxylate transporters MCT1 and MCT2 that binds to an intracellular site involving transmembrane helices 7–10. *Biochem. J.* **425**, 523–530. <https://doi.org/10.1042/BJ20091515>.
59. Ovens, M.J., Manoharan, C., Wilson, M.C., Murray, C.M., and Halestrap, A.P. (2010). The inhibition of monocarboxylate transporter 2 (MCT2) by AR-C155858 is modulated by the associated ancillary protein. *Biochem. J.* **431**, 217–225. <https://doi.org/10.1042/BJ20100890>.
60. Xu, Y., Pan, X., Hu, S., Zhu, Y., Cassim Bawa, F., Li, Y., Yin, L., and Zhang, Y. (2021). Hepatocyte-specific expression of human carboxylesterase 2 attenuates nonalcoholic steatohepatitis in mice. *Am. J. Physiol. Gastrointest. Liver Physiol.* **320**, G166–G174. <https://doi.org/10.1152/ajpgi.00315.2020>.
61. Li, Y., Zalzal, M., Jadhav, K., Xu, Y., Kasumov, T., Yin, L., and Zhang, Y. (2016). Carboxylesterase 2 prevents liver steatosis by modulating lipolysis, endoplasmic reticulum stress, and lipogenesis and is regulated by hepatocyte nuclear factor 4 alpha in mice. *Hepatology* **63**, 1860–1874. <https://doi.org/10.1002/hep.28472>.
62. Ruby, M.A., Massart, J., Hunerdosse, D.M., Schonke, M., Correia, J.C., Louie, S.M., Ruas, J.L., Naslund, E., Nomura, D.K., and Zierath, J.R. (2017). Human carboxylesterase 2 reverses obesity-induced diacylglycerol accumulation and glucose intolerance. *Cell Rep.* **18**, 636–646. <https://doi.org/10.1016/j.celrep.2016.12.070>.
63. Maresch, L.K., Benedikt, P., Feiler, U., Eder, S., Zierler, K.A., Taschler, U., Kolleritsch, S., Eichmann, T.O., Schoiswohl, G., Leopold, C., et al. (2019). Intestine-specific overexpression of carboxylesterase 2c protects mice from diet-induced liver steatosis and obesity. *Hepatol. Commun.* **3**, 227–245. <https://doi.org/10.1002/hep4.1292>.
64. Hsieh, Y.T., Lin, H.P., Chen, B.M., Huang, P.T., and Roffler, S.R. (2015). Effect of cellular location of human carboxylesterase 2 on CPT-11 hydrolysis and anticancer activity. *PLoS One* **10**, e0141088. <https://doi.org/10.1371/journal.pone.0141088>.
65. Oosterhoff, D., Overmeer, R.M., de Graaf, M., van der Meulen, I.H., Giaccone, G., van Beusechem, V.W., Haisma, H.J., Pinedo, H.M., and Geritsen, W.R. (2005). Adenoviral vector-mediated expression of a gene encoding secreted, EpCAM-targeted carboxylesterase-2 sensitizes colon cancer spheroids to CPT-11. *Br. J. Cancer* **92**, 882–887. <https://doi.org/10.1038/sj.bjc.6602362>.
66. Potter, P.M., Wolverson, J.S., Morton, C.L., Wierdl, M., and Danks, M.K. (1998). Cellular localization domains of a rabbit and a human carboxylesterase: influence on irinotecan (CPT-11) metabolism by the rabbit enzyme. *Cancer Res.* **58**, 3627–3632.
67. Raun, S.H., Henriquez-Olguin, C., Karavaeva, I., Ali, M., Moller, L.L.V., Kot, W., Castro-Mejia, J.L., Nielsen, D.S., Gerhart-Hines, Z., Richter, E.A., and Sylow, L. (2020). Housing temperature influences exercise training adaptations in mice. *Nat. Commun.* **11**, 1560. <https://doi.org/10.1038/s41467-020-15311-y>.
68. Møller, L.L.V., Raun, S.H., Fritzen, A.M., and Sylow, L. (2022). Measurement of skeletal muscle glucose uptake in mice in response to acute treadmill running. *J. Biol. Methods* **9**, e162. <https://doi.org/10.14440/jbm.2022.385>.
69. Raven, A., Lu, W.Y., Man, T.Y., Ferreira-Gonzalez, S., O'Duibhir, E., Dwyer, B.J., Thomson, J.P., Meehan, R.R., Bogorad, R., Kotlianski,

- V., et al. (2017). Cholangiocytes act as facultative liver stem cells during impaired hepatocyte regeneration. *Nature* 547, 350–354. <https://doi.org/10.1038/nature23015>.
70. Wang, G., Chow, R.D., Ye, L., Guzman, C.D., Dai, X., Dong, M.B., Zhang, F., Sharp, P.A., Platt, R.J., and Chen, S. (2018). Mapping a functional cancer genome atlas of tumor suppressors in mouse liver using AAV-CRISPR-mediated direct in vivo screening. *Sci. Adv.* 4, eaao5508. <https://doi.org/10.1126/sciadv.aao5508>.
71. Guijas, C., Montenegro-Burke, J.R., Domingo-Almenara, X., Palermo, A., Warth, B., Hermann, G., Koellensperger, G., Huan, T., Uritboonthai, W., Aisporna, A.E., et al. (2018). METLIN: a technology platform for identifying knowns and unknowns. *Anal. Chem.* 90, 3156–3164. <https://doi.org/10.1021/acs.analchem.7b04424>.
72. De Nardo, W., Miotto, P.M., Bayliss, J., Nie, S., Keenan, S.N., Montgomery, M.K., and Watt, M.J. (2022). Proteomic analysis reveals exercise training induced remodelling of hepatokine secretion and uncovers syndecan-4 as a regulator of hepatic lipid metabolism. *Mol. Metab.* 60, 101491. <https://doi.org/10.1016/j.molmet.2022.101491>.
73. Yang, J., Vamvini, M., Nigro, P., Ho, L.L., Galani, K., Alvarez, M., Tanigawa, Y., Renfro, A., Carbone, N.P., Laakso, M., et al. (2022). Single-cell dissection of the obesity-exercise axis in adipose-muscle tissues implies a critical role for mesenchymal stem cells. *Cell Metab.* 34, 1578–1593.e6. <https://doi.org/10.1016/j.cmet.2022.09.004>.
74. Shin, S., Pang, Y., Park, J., Liu, L., Lukas, B.E., Kim, S.H., Kim, K.W., Xu, P., Berry, D.C., and Jiang, Y. (2020). Dynamic control of adipose tissue development and adult tissue homeostasis by platelet-derived growth factor receptor alpha. *eLife* 9, e56189. <https://doi.org/10.7554/eLife.56189>.
75. Guseh, J.S., Churchill, T.W., Yeri, A., Lo, C., Brown, M., Houstis, N.E., Aragam, K.G., Lieberman, D.E., Rosenzweig, A., and Baggish, A.L. (2020). An expanded repertoire of intensity-dependent exercise-responsive plasma proteins tied to loci of human disease risk. *Sci. Rep.* 10, 10831. <https://doi.org/10.1038/s41598-020-67669-0>.
76. Tang, S., Beattie, A.T., Kafkova, L., Petris, G., Huguenin-Dezot, N., Fiedler, M., Freeman, M., and Chin, J.W. (2022). Mechanism-based traps enable protease and hydrolase substrate discovery. *Nature* 602, 701–707. <https://doi.org/10.1038/s41586-022-04414-9>.
77. Wilkinson, S.B., Phillips, S.M., Atherton, P.J., Patel, R., Yarasheski, K.E., Tarnopolsky, M.A., and Rennie, M.J. (2008). Differential effects of resistance and endurance exercise in the fed state on signalling molecule phosphorylation and protein synthesis in human muscle. *J. Physiol.* 586, 3701–3717. <https://doi.org/10.1113/jphysiol.2008.153916>.
78. Kraemer, W.J., and Ratamess, N.A. (2005). Hormonal responses and adaptations to resistance exercise and training. *Sports Med.* 35, 339–361. <https://doi.org/10.2165/00007256-200535040-00004>.
79. Robbins, J.M., Peterson, B., Schraner, D., Tahir, U.A., Rienmuller, T., Deng, S., Keyes, M.J., Katz, D.H., Beltran, P.M.J., Barber, J.L., et al. (2021). Human plasma proteomic profiles indicative of cardiorespiratory fitness. *Nat. Metab.* 3, 786–797. <https://doi.org/10.1038/s42255-021-00400-z>.
80. Sanford, J.A., Nogiec, C.D., Lindholm, M.E., Adkins, J.N., Amar, D., Dasari, S., Drugan, J.K., Fernandez, F.M., Radom-Aizik, S., Schenk, S., et al. (2020). Molecular Transducers of Physical Activity Consortium (MoTrPAC): mapping the dynamic responses to exercise. *Cell* 181, 1464–1474. <https://doi.org/10.1016/j.cell.2020.06.004>.
81. Sato, S., Basse, A.L., Schonke, M., Chen, S., Samad, M., Altıntaş, A., Laker, R.C., Dalbram, E., Barres, R., Baldi, P., et al. (2019). Time of exercise specifies the impact on muscle metabolic pathways and systemic energy homeostasis. *Cell Metab.* 30, 92–110.e4. <https://doi.org/10.1016/j.cmet.2019.03.013>.
82. Ezagouri, S., Zwighaft, Z., Sobel, J., Baillieu, S., Doutreleau, S., Ladeuix, B., Golik, M., Verges, S., and Asher, G. (2019). Physiological and molecular dissection of daily variance in exercise capacity. *Cell Metab.* 30, 78–91.e4. <https://doi.org/10.1016/j.cmet.2019.03.012>.
83. Pendergrast, L.A., Lundell, L.S., Ehrlich, A.M., Ashcroft, S.P., Schonke, M., Basse, A.L., Krook, A., Treebak, J.T., Dollet, L., and Zierath, J.R. (2023). Time of day determines postexercise metabolism in mouse adipose tissue. *Proc. Natl. Acad. Sci. USA* 120, e2218510120. <https://doi.org/10.1073/pnas.2218510120>.
84. Gombash Lampe, S.E., Kaspar, B.K., and Foust, K.D. (2014). Intravenous injections in neonatal mice. *JoVE* 52037. <https://doi.org/10.3791/52037>.
85. Amodei, D., Egertson, J., MacLean, B.X., Johnson, R., Merrihew, G.E., Keller, A., Marsh, D., Vitek, O., Mallick, P., and MacCoss, M.J. (2019). Improving precursor selectivity in data-independent acquisition using overlapping windows. *J. Am. Soc. Mass Spectrom.* 30, 669–684. <https://doi.org/10.1007/s13361-018-2122-8>.
86. Perez-Riverol, Y., Bai, J., Bandla, C., Garcia-Seisdedos, D., Hewapathirana, S., Kamatchinathan, S., Kundu, D.J., Prakash, A., Frericks-Zipper, A., Eisenacher, M., et al. (2022). The PRIDE database resources in 2022: a hub for mass spectrometry-based proteomics evidences. *Nucleic Acids Res.* 50, D543–D552. <https://doi.org/10.1093/nar/gkab1038>.
87. Adusumilli, R., and Mallick, P. (2017). Data conversion with ProteoWizard msConvert. *Methods Mol. Biol.* 1550, 339–368. https://doi.org/10.1007/978-1-4939-6747-6_23.
88. Ting, Y.S., Egertson, J.D., Bollinger, J.G., Searle, B.C., Payne, S.H., Noble, W.S., and MacCoss, M.J. (2017). PECAN: library-free peptide detection for data-independent acquisition tandem mass spectrometry data. *Nat. Methods* 14, 903–908. <https://doi.org/10.1038/nmeth.4390>.
89. UniProt Consortium (2021). UniProt: the universal protein knowledgebase in 2021. *Nucleic Acids Res.* 49, D480–D489. <https://doi.org/10.1093/nar/gkaa1100>.
90. Mellacheruvu, D., Wright, Z., Couzens, A.L., Lambert, J.P., St-Denis, N.A., Li, T., Miteva, Y.V., Hauri, S., Sardi, M.E., Low, T.Y., et al. (2013). The CRAPome: a contaminant repository for affinity purification-mass spectrometry data. *Nat. Methods* 10, 730–736. <https://doi.org/10.1038/nmeth.2557>.
91. Bourgon, R., Gentleman, R., and Huber, W. (2010). Independent filtering increases detection power for high-throughput experiments. *Proc. Natl. Acad. Sci. USA* 107, 9546–9551. <https://doi.org/10.1073/pnas.0914005107>.
92. Ashburner, M., Ball, C.A., Blake, J.A., Botstein, D., Butler, H., Cherry, J.M., Davis, A.P., Dolinski, K., Dwight, S.S., Eppig, J.T., et al. (2000). Gene ontology: tool for the unification of biology. The Gene Ontology Consortium. *Nat. Genet.* 25, 25–29. <https://doi.org/10.1038/75556>.
93. Jiang, Z., Zhao, M., Voilquin, L., Jung, Y., Aikio, M.A., Sahai, T., Dou, F.Y., Roche, A.M., Carcamo-Orive, I., Knowles, J.W., et al. (2021). Isthmin-1 is an adipokine that promotes glucose uptake and improves glucose tolerance and hepatic steatosis. *Cell Metab.* 33, 1836–1852.e11. <https://doi.org/10.1016/j.cmet.2021.07.010>.
94. Li, V.L., He, Y., Contrepois, K., Liu, H., Kim, J.T., Wiggernhorn, A.L., Tanzo, J.T., Tung, A.S.H., Lyu, X., Zushin, P.J.H., et al. (2022). An exercise-inducible metabolite that suppresses feeding and obesity. *Nature* 606, 785–790. <https://doi.org/10.1038/s41586-022-04828-5>.
95. Smith, C.A., Want, E.J., O'Maille, G., Abagyan, R., and Siuzdak, G. (2006). XCMS: processing mass spectrometry data for metabolite profiling using nonlinear peak alignment, matching, and identification. *Anal. Chem.* 78, 779–787. <https://doi.org/10.1021/ac051437y>.
96. Ross, M.K., and Borazjani, A. (2007). Enzymatic activity of human carboxylesterases. *Curr. Protoc. Toxicol. Chapter 4. Unit 4.24*. <https://doi.org/10.1002/0471140856.tx0424s33>.
97. Alvarez-Castelao, B., Schanzenbacher, C.T., Hanus, C., Glock, C., Tom Dieck, S., Dorrbaum, A.R., Bartnik, I., Nassim-Assir, B., Ciiradaeva, E., Mueller, A., et al. (2017). Cell-type-specific metabolic labeling of nascent proteomes in vivo. *Nat. Biotechnol.* 35, 1196–1201. <https://doi.org/10.1038/nbt.4016>.

98. Ritchie, M.E., Phipson, B., Wu, D., Hu, Y., Law, C.W., Shi, W., and Smyth, G.K. (2015). limma powers differential expression analyses for RNA-sequencing and microarray studies. *Nucleic Acids Res.* 43, e47. <https://doi.org/10.1093/nar/gkv007>.
99. Law, C.W., Alhamdoosh, M., Su, S., Dong, X., Tian, L., Smyth, G.K., and Ritchie, M.E. (2016). RNA-seq analysis is easy as 1-2-3 with limma, Glimma and edgeR. *F1000Res.* 5. <https://doi.org/10.12688/f1000research.9005.3>.
100. Smyth, G.K. (2004). Linear models and empirical bayes methods for assessing differential expression in microarray experiments. *Stat. Appl. Genet. Mol. Biol.* 3, Article3. <https://doi.org/10.2202/1544-6115.1027>.

STAR★METHODS

KEY RESOURCES TABLE

REAGENT or RESOURCE	SOURCE	IDENTIFIER
Antibodies		
Anti-V5 antibody (1:1000 dilution)	Invitrogen	Cat# R960-25; RRID: AB_2556564
Anti-Flag antibody (1:1000 dilution)	Sigma	Cat# F1804; RRID: AB_262044
Anti- β Tubulin (1:5000 dilution)	Abcam	Cat# ab6046; RRID: AB_2210370
Anti-CES2 (1:1000 dilution)	Novus Biologicals	Cat# NBP1-91620; RRID: AB_11025437
Anti-TIMP3 (1:500 dilution)	Thermo Fisher	Cat# 710404; RRID: AB_2532709
Anti-F13A (1:500 dilution)	MyBioSource	MBS2026456
Anti-ITIH2 (1:500 dilution)	MyBioSource	MBS9612213
Anti-C4BPA (1:500 dilution)	Abnova	Cat# H00000722-D01P; RRID: AB_1673096
Anti-mouse IgG IRDye 680RD (1:10000 dilution)	LI-COR	Cat# 925-68070; RRID: AB_2651128
Anti-rabbit IgG IRDye 800RD (1:10000 dilution)	LI-COR	Cat# 926-32211; RRID: AB_621843
Anti-biotin Streptavidin Alexa Fluor 680 (1:1000 dilution)	ThermoFisher	S32358
FITC anti-Mouse TCR β	BioLegend	Cat# 109206; RRID: AB_313429
PerCP/Cy5.5 anti-Mouse CD19 antibody	BioLegend	Cat# 152406; RRID: AB_2629815
Anti-mouse albumin (1:5000 dilution)	Novus Biologicals	Cat# NB600-41532; RRID: AB_805588
Anti-BHMT (1:1000 dilution)	Abcam	Cat# ab96415; RRID: AB_10697919
Anti-goat IgG IRDye 800CW (1:10000 dilution)	LI-COR	Cat# 925-32214; RRID: AB_2687553
Bacterial and virus strains		
One Shot TOP10 Chemically Competent <i>E. coli</i>	Invitrogen	C404010
AAV9-FLEX-ER-TurboID	UPenn Vector Core	60221S
AAV8- <i>Tbg</i> -GFP	Addgene	105535-AAV8
AAV8- <i>Tbg</i> -CES2A- Δ C	UPenn Vector Core	63849S
AAV8- <i>Tbg</i> -CES2C- Δ C	UPenn Vector Core	63850S
AAV8- <i>Tbg</i> -CES2A- Δ C-S227A	UPenn Vector Core	V7929S
AAV8- <i>Tbg</i> -CES2C- Δ C-S230A	UPenn Vector Core	V7928S
Chemicals, peptides, and recombinant proteins		
Biotin	Sigma	B4501-1G
DTT	Sigma	D0632-1G
4-nitrophenyl acetate	Sigma	N8130-5G
D-(+)-Glucose	Sigma	50-99-7
DPBS	Thermo Fisher	14190144
Human recombinant insulin	Sigma	91077C
Dexamethasone	Sigma	D4902-100MG
Rosiglitazone	Cayman	71740
IBMX	Sigma	I-5879
BSA	Sigma	A7906-500G
Sodium azide	Sigma	S2002-25G
Sodium chloride	Sigma	S9888-500G
Sodium deoxycholate	Sigma	D6750-100G
Sodium dodecyl sulfate	Thermo Fisher	BP166-500
Sodium carbonate	Thermo Fisher	S263-500
Sodium bicarbonate	Thermo Fisher	187508
Sodium ascorbate	Thermo Fisher	A0539500G
Sodium L-lactate	Sigma	L7022-5G
Sodium fumarate dibasic	Sigma	F1506-25G

(Continued on next page)

<i>Continued</i>		
REAGENT or RESOURCE	SOURCE	IDENTIFIER
Sodium succinate dibasic hexahydrate	Sigma	S2378-100G
Sodium (R)-3-hydroxybutyrate	Sigma	298360-1G
Kynurenic acid	Sigma	K3375-250MG
D-Pantothenic acid hemicalcium salt	Sigma	21210-5G-F
Sodium pyruvate	Sigma	P2256-25G
L-(–)-Malic acid	Sigma	02288-10G
Dimethyl sulfoxide	Sigma	D8418-100ML
Potassium chloride	Sigma	P3911-500G
EDTA	Sigma	E9884-100G
EDTA, 0.5 M, pH 8.0	EMD Millipore	324506
Tris-HCl	Sigma	1185-53-1
Acetonitrile	Thermo Fisher	A998-4
Alcohol ethyl ethanol 200 proof	Gold Shield Distributors	0412804-PINT
HALT protease inhibitor	Thermo Fisher	78429
NP-40 alternative	Millipore	492016-100ML
Chloroform	Thermo Fisher	C607-4
Ponceau S solution	Sigma	P7170-1L
NuPAGE MOPS SDS Running Buffer (20X)	Invitrogen	NP0001-02
NuPAGE 4–12% Bis-Tris Protein Gels, 1.0 mm, 15-well	Thermo Fisher	NP0323BOX
Odyssey blocking buffer	LI-COR	927–50000
Seeblue plus 2 protein ladder	Thermo Fisher	LC5925
NuPAGE LDS Sample Buffer (4X)	Thermo Fisher	NP0008
Urea	Sigma	31K0038
Acetone	Thermo Fisher	A184
Formic acid	Thermo Fisher	A117-50
Phosphoric acid	Sigma	345245-100ML
Trolox	Sigma	648471-500MG
0.9% saline solution	Teknova	S5825
TEAB solution (1M)	Sigma	T7408-100ML
Kolliphor EL	Sigma	C5135-500G
Pierce 16% Formaldehyde (w/v), Methanol-free	Thermo Fisher	28908
Trypsin	Promega	V5113
Iodoacetamide	Sigma	A3221
Brefeldin A0	Sigma	B6542-5MG
AR-C155858	Tocris	4960
<i>Critical commercial assays</i>		
SilverQuest Silver Staining Kit	Thermo Fisher	LC6070
Trans-blot turbo RTA transfer kit, nitrocellulose	Biorad	1704271
LIVE/DEAD Fixable Aqua Dead Cell Stain Kit	Invitrogen	L34957
RNeasy Mini Kit	Qiagen	74106
Q5 Site-Directed Mutagenesis Kit	NEB Biolabs	E0554S
High-Capacity cDNA Reverse Transcription Kit	Thermo Fisher	4368813
<i>Deposited data</i>		
Proteomic data	This study	ProteomeXchange: PXD021602
Processed proteomic datasets	This study	Table S1
<i>Experimental models: Cell lines</i>		
HEK293T cells	ATCC	CRL-3216
Primary mouse hepatocytes	This paper	N/A

(Continued on next page)

Continued

REAGENT or RESOURCE	SOURCE	IDENTIFIER
Experimental models: Organisms/strains		
C57BL/6J (<i>M. musculus</i>)	Jackson Laboratory	000664
<i>Alb</i> -cre mice	Jackson Laboratory	003574
<i>Cdh16</i> -cre mice	Jackson Laboratory	012237
<i>Gcg</i> -icre mice	Jackson Laboratory	030663
<i>Pdx1</i> -cre mice	Jackson Laboratory	014647
<i>Myh6</i> -creER mice	Jackson Laboratory	005657
<i>MCK</i> -cre mice	Jackson Laboratory	006475
<i>Myh11</i> -icreER mice	Jackson Laboratory	019079
<i>Cdh5</i> -cre mice	Jackson Laboratory	006137
<i>Pdgfra</i> -creER mice	Jackson Laboratory	032770
<i>Pdgfrb</i> -creER mice	Jackson Laboratory	030201
<i>Vil1</i> -cre mice	Jackson Laboratory	021504
<i>Sftpc</i> -creER mice	Jackson Laboratory	028054
<i>Col1a1</i> -creER mice	Jackson Laboratory	016241
<i>CD2</i> -icre mice	Jackson Laboratory	008520
<i>Lck</i> -cre mice	Jackson Laboratory	003802
<i>Nr5a1</i> -cre mice	Jackson Laboratory	033687
<i>Nes</i> -creER mice	Jackson Laboratory	016261
<i>Syn1</i> -cre mice	Jackson Laboratory	003966
<i>Adipoq</i> -cre mice	Jackson Laboratory	028020
<i>Ucp1</i> -cre mice	Jackson Laboratory	024670
<i>LysM</i> -creER mice	Jackson Laboratory	032291
Oligonucleotides		
See Table S7	N/A	N/A
Recombinant DNA		
pAAV-FLEX-ER-TurboID plasmid	Addgene	160857
pAAV- <i>Tbg</i> -ER-TurboID plasmid	Addgene	149415
pDEST40-CES2A-ΔC expression plasmid	This paper	Addgene 200554
pDEST40-CES2C-ΔC expression plasmid	This paper	Addgene 200555
pDEST40-CES2A-ΔC-S227A expression plasmid	This paper	Addgene 200556
pDEST40-CES2C-ΔC-S230A expression plasmid	This paper	Addgene 200557
pAAV- <i>Tbg</i> -CES2A-ΔC plasmid	This paper	Addgene 200558
pAAV- <i>Tbg</i> -CES2C-ΔC plasmid	This paper	Addgene 200559
pAAV- <i>Tbg</i> -CES2A-ΔC-S227A plasmid	This paper	Addgene 200560
pAAV- <i>Tbg</i> -CES2C-ΔC-S230A plasmid	This paper	Addgene 200561
Other		
3 kDa Molecular Weight Cutoff Filter	Amicon	UFC9003
pENTR/D-TOPO Cloning Kit	Invitrogen	K240020
Gateway LR Clonase Enzyme mix	Invitrogen	11791019
Gibson Assembly Master Mix	NEB Biolabs	E2611L
Phusion High-Fidelity PCR Master Mix with HF Buffer	NEB Biolabs	M0531L
ExpiFectamine 293 Transfection Kit	Thermo Fisher	A14524
His GraviTrap TALON	Cytiva	29-0005-94
QIAquick gel extraction kit	Qiagen	28704
EndoFree Plasmid Maxi Kit	Qiagen	12362
NotI	NEB Biolabs	R3189S
HindIII	NEB Biolabs	R3104S
EcoRV	NEB Biolabs	R3195S

(Continued on next page)

Continued

REAGENT or RESOURCE	SOURCE	IDENTIFIER
Xhol	NEB Biolabs	R0146S
HFD with 60 kcal% fat	ResearchDiets	D12492
Thioglycollate Medium Brewer Modified	Thermo Fisher	B11716
Collagen I, Rat	Corning	CB-40236
Dispase II	Roche	04942078001
Collagenase D	Roche	11088882001
Collagenase IV	Sigma	C5138-1G
Percoll	Sigma	P4937-500ML
10x PBS	Gibco	70011044
HBSS buffer	Gibco	14175-095
Williams E media	Quality Biological	10128-636
Corning Regular Fetal Bovine Serum	Corning	35-010-CV
DMEM	Corning	10-017-CV
DMEM/F12 (1:1)	Gibco	11320082
DMEM/F-12, GlutaMAX supplement	Gibco	10565042
Expi293 Expression medium	Thermo Fisher	A1435101
100um cell strainer	Falcon	352360
70um cell strainer	Falcon	352350
S-Trap micro columns	Protifi	C02-micro-80
lithium heparin tube	BD	365985
PrecisionGlide Needle 21G	BD	305129
Exel International Insulin Syringes 29G	Exel International	14-841-32
Ultrafine Insulin Syringes 31G	BD	328290
Trypan blue solution 0.4%	Invitrogen	15250061
Ultra Sensitive Mouse Insulin ELISA Kit	Crystal Chem	90080
Triglyceride colorimetric assay kit	Cayman	10010303
Pierce BCA Protein Assay Kit	Thermo Fisher	23225
Tailveiner Restraint for Mice	Braintree	TV-150 STD
Streptavidin magnetic beads	Thermo Fisher	65601
Blood Glucose meter	OneTouch Ultra-Mini meter	N/A
Blood Glucose Strips	GenUltimate	100-50
96-Well Microplate Fisherbrand	Fisher Scientific	12565501
TRIzol Reagent	Invitrogen	15596026
Ssoadvance Universal SYBR Green mix	Biorad	1725272
Bulk tubes	Thermo Fisher	15340162
Metal Bulk Beads	Thermo Fisher	15340158
Benchmark BeadBlaster Homogenizer	Thermo Fisher	15-340-163
Orbitrap Fusion Tribrid Mass Spectrometer	Thermo Fisher	N/A
Agilent 6470 triple quadrupole LC-MS instrument	Agilent	N/A
NH2 100 Å LC column	Phenomenex	00B-4378-E0

RESOURCE AVAILABILITY

Lead contact

Further information and requests for reagents may be directed to and will be fulfilled by the lead contact Dr. Jonathan Z. Long (jzlong@stanford.edu).

Materials availability

Further information and requests for reagents will be fulfilled by Dr. Jonathan Z. Long (jzlong@stanford.edu). A list of critical reagents (key resources) is included in the [key resources table](#). Material that can be shared will be released via a Material Transfer Agreement.

Data and code availability

- The mass spectrometry proteomics data have been deposited to the ProteomeXchange Consortium via the PRIDE partner repository with the dataset identifier PXD034535. Processed data from these outputs are available as [supplemental information](#) files. Uncropped blots and values of graphs are included in the zip file, [Data S1](#).
- This paper does not report original code.
- Any additional information required to reanalyze the data reported in this paper is available from the lead contact upon request.

EXPERIMENTAL MODEL AND SUBJECT DETAILS

Mouse models

Animal experiments were performed according to procedures approved by the Stanford University IACUC. Mice were maintained in 12 h light-dark cycles at 22°C and ~50% relative humidity and fed a standard irradiated rodent chow diet. Where indicated, high fat diet (Research Diets, D12492) was used. C57BL/6J male and female mice (stock no. 000664), homozygous *Alb*-cre male mice (stock no. 003574), hemizygous *Cdh16*-cre male mice (stock no. 012237), homozygous *Gcg*-cre male mice (stock no. 030663), hemizygous *Pdx1*-cre male mice (stock no. 014647), homozygous *Myh6*-creER male mice (stock no. 005657), hemizygous *MCK*-cre male mice (stock no. 006475), hemizygous *Myh11*-creER male mice (stock no. 019079), homozygous *Cdh5*-cre male mice (stock no. 006137), heterozygous *Pdgfra*-creER male and female mice (stock no. 032770), homozygous *Pdgfrb*-creER male mice (stock no. 030201), hemizygous *Vil1*-cre male mice (stock no. 021504), homozygous *Sftpc*-creER male mice (stock no. 028054), hemizygous *Col1a1*-creER male mice (stock no. 016241), hemizygous *CD2*-cre male mice (stock no. 008520), hemizygous *Lck*-cre male mice (stock no. 003802), hemizygous *Nr5a1*-creER male mice (stock no. 033687), hemizygous *Nes*-creER male mice (stock no. 016261), hemizygous *Syn1*-cre male mice (stock no. 003966), hemizygous *Adipoq*-cre male mice (stock no. 028020), hemizygous *Ucp1*-cre male mice (stock no. 024670), and hemizygous *LysM*-cre male mice (stock no. 031674) were purchased from Jackson Laboratory. All the cre driver male mice were crossed with female C57BL/6J mice to generate hemizygous/heterozygous mice. Genotypes were verified following genotyping protocols and using the primers listed on the Jackson Laboratory website. The reported Cre tissue expression pattern from Jackson Laboratory and detected tissue expression was shown in [Table S5](#).

METHOD DETAILS

Cell line cultures

HEK293T cells were obtained from ATCC (CRL-3216) and cultured in complete medium (Dulbecco's Modified Eagle's Medium, Corning, 10013CV; 10% FBS, Corning, 35010CV; 1:1,000 penicillin-streptomycin, Gibco, 15140-122). Cells were grown at 37°C with 5% CO₂. For transient transfection, cells were transfected in 10 cm² at ~60% confluency using PolyFect (Qiagen, 301107) and washed with complete medium 6 h later.

Western blotting

For analyzing samples using Western blot, proteins were separated on NuPAGE 4–12% Bis-Tris gels and transferred to nitrocellulose membranes. Equal loading was ensured by staining blots with Ponceau S solution. Blots were then incubated with Odyssey blocking buffer for 30 min at room temperature and incubated with primary antibodies (1:1000 dilution mouse anti-V5 antibody (Invitrogen, R960-25), 1:1000 dilution mouse anti-FLAG antibody (Sigma, F1804), 1:5000 dilution rabbit anti-β-tubulin antibody (Abcam, ab6046), 1:1000 dilution rabbit anti-CES2 antibody (Novus Biologicals, NBP1-91620), 1:500 rabbit anti-TIMP3 antibody (Thermo Fisher, 710404), 1:500 rabbit anti-F13A antibody (MyBioSource, MBS2026456), 1:500 rabbit anti-ITIH2 (MyBioSource, MBS9612213), 1:500 dilution rabbit anti-C4BPA (Abnova, H00000722D01P), 1:5000 dilution goat anti-albumin antibody (Novus biological, NB600-41532), 1:1000 dilution rabbit anti-H6PD antibody (Abcam, ab170895), 1:1000 dilution rabbit anti-BHMT (Abcam, ab96415), 1:1000 dilution streptavidin Alexa Fluor 680 (Thermo Fisher, S32358)) in blocking buffer overnight at 4°C. Blots were washed three times with PBST (0.05% Tween 20 in PBS) and stained with species-matched secondary antibodies (1:10000 dilution goat anti-mouse IRDye 680RD (LI-COR, 925–68070), 1:10000 dilution goat anti-rabbit IRDye 800RD (LI-COR, 925–68070), 1:10000 dilution donkey anti-goat IRDye 800CW (LI-COR, 925–32214)) at room temperature for 1 h. Blots were further washed three times with PBST and imaged with the Odyssey CLx Imaging System. Secondary antibodies were not required for imaging blots incubated with streptavidin Alexa Fluor 680 primary antibody.

AAV production

pAAV-FLEX-ER-TurboID (Addgene, 160857), pAAV-*Tbg*-CES2A-ΔC, pAAV-*Tbg*-CES2C-ΔC, pAAV-*Tbg*-CES2A-ΔC-S227A and pAAV-*Tbg*-CES2C-ΔC-S230A plasmids were amplified, extracted using an endotoxin-free Qiagen Maxiprep kit (Qiagen, 12362) and sequence verified. AAV9-FLEX-ER-TurboID (60221S), AAV8-*Tbg*-CES2A-ΔC (63849S), AAV8-*Tbg*-CES2C-ΔC (63850S), AAV8-*Tbg*-CES2A-ΔC-S227A (V7929S) and AAV8-*Tbg*-CES2C-ΔC-S230A (V7928S) viruses were made with Penn Vector Core.

Viral transduction

For transduction of brain-specific cre driver lines (*Syn1-cre* and *Nes-creER* mice), injection was carried out as previously reported.⁸⁴ Briefly, postnatal day 1 pups were anesthetized on ice for 30–60 s. The temporal vein was identified under a dissection microscope and injected with $10e11$ genome copies (GC) of AAV9-FLEX-ER-TurboID virus per mouse diluted in a total volume of 30 μ L saline (containing 0.3 μ L 0.4% Trypan blue solution) with a 31G syringe (BD, 328290). Injected pups were then recovered in hands for 30 s and returned to home cages. For *Syn1-cre* mice, 8 to 9 weeks after injection, 1-week treadmill running was performed as described below on male mice with the correct genotype. For *Nes-creER* mice, 5 to 6 weeks after injection. Tamoxifen (Sigma, T5648-1G) was prepared as a 20 mg/mL solution in corn oil and administered daily for 5 days (100 μ L per day, intraperitoneally) to induce recombination. 3 weeks after the final tamoxifen injection, 1-week treadmill running was performed on male mice with the correct genotype. For transduction of cre/ice driver mice (except *Syn1-cre* mice), 6-week-old male hemizygous mice were injected via tail vein with a 29G syringe (Thermo Fisher, 14-841-32) at a dose of $3 \times 10e11$ GC per mouse diluted in saline in a total volume of 100 μ L per mouse. Three weeks after transduction with the AAV9-FLEX-ER-TurboID virus, 1-week treadmill running was performed. For transduction of creER/iceER mice (except *Nes-creER* mice), AAV9-FLEX-ER-TurboID virus was injected via tail vein into 6-week-old hemizygous/heterozygous male mice at a dose of $3 \times 10e11$ GC per mouse. After a 2-week transduction period, tamoxifen (Sigma, T5648-1G) was prepared as a 20 mg/mL solution in corn oil and administered daily for 5 days (100 μ L per day, intraperitoneally) to induce recombination. After the final tamoxifen injection, mice were housed in their home cages for 3 additional weeks before performing 1-week treadmill running. For transduction of C57BL/6J mice, AAV8-*Tbg*-CES2A- Δ C/CES2C- Δ C/GFP viruses were injected via tail vein into 8 to 10-week-old male mice at a dose of $10e11$ GC per mouse. One week after viral transduction, mice were fed with HFD (60% fat, Research Diets, D12492). Body weights and food intake were measured every week. After 6 weeks of HFD feeding, glucose tolerance and insulin tolerance tests were performed. At the end of 7 weeks of HFD feeding, tissues and blood were collected for further analysis.

Mouse exercise and secretome labeling protocols

A 6-lane animal treadmill (Columbus Instruments, 1055-SRM-D65) was used for mouse running. Prior to treadmill running, the body-weight of individual mice was measured with a tabletop scale. Mice were then acclimated to the treadmill for 5 min before running at a speed of 5 m/min for 5 min. Then the speed was increased to 20 m/min and kept constant for 60 min. A serological pipette was used to manually stir the mice to avoid excessive electrical shock during the whole running period. After exercise, mice were returned to home cages. The sedentary control animals were kept in their home cages but removed from the original racks and put next to the treadmill. These mice were constantly disturbed by the noises from the running animals and treadmill. Running was performed for 7 consecutive days in the morning (between 9 and 12 a.m.). On the fourth day of one-week treadmill running, biotin water (0.5 mg/mL) was supplemented to initiate labeling and kept accessible to mice until the end of the experiment. On the next day, an additional dose of biotin was administered by injection (24 mg/mL, intraperitoneally, in a solution of 18:1:1 saline:Kolliphor EL:DMSO, final volume of 200 μ L per mouse per day) 1 h prior to the running for 3 consecutive days. Sedentary animals received biotin delivery the same as exercise animals.

Quantitative PCR

We collected the following tissues from the indicated genotypes: liver from *Alb-cre* mice, heart from *Myh6-creER* and *Myh11-iceER* mice, brain from *Syn1-cre* and *Nes-creER* mice, iWAT from *Adipoq-cre* mice, BAT from *Ucp1-cre* mice, lung from *Sftpc-creER*, *Pdgfr α -creER*, *Pdgfr β -creER* and *Cdh5-cre* mice, quadriceps muscle from *MCK-cre* mice, intestines from *Vil1-cre* mice, pancreas from *Gcg-ice* and *Pdx1-cre* mice, kidney from *Cdh16-cre* mice, adrenal gland from *Nr5a1-cre* mice, hindlimb with muscles removed from *Col1a1-creER* mice. For *Lck-cre* and *CD2-ice* mice, splenocytes were collected by passing the spleen through a cell strainer (Corning, 352350) and resuspended in 2% BSA solution. Splenocytes were stained with FITC anti-mouse TCR β (BioLegend, 109206), Percp/Cy5.5 anti-mouse CD19 (BioLegend, 152406) and LIVE/DEAD Aqua (Invitrogen, L34957). $\alpha\beta$ T cells from *Lck-cre* mice were gated on Aqua-CD19-TCR β +, isolated with FACS, and spun down at 300 g for 5 min at 4°C for downstream analysis. For *CD2-ice* mice, $\alpha\beta$ T cells were gated on Aqua-CD19-TCR β + and B cells were gated on Aqua-CD19+TCR β -. Both $\alpha\beta$ T cells and B cells were sorted with FACS, mixed, and spun down at 300 g for 5 min at 4°C for downstream analysis. For *Lysm-creER* mice, a new cohort of 6 to 8-week old mice ($n = 3$) was transduced with AAV9-FLEX-ER-TurboID virus and was injected with tamoxifen to induce cre recombination the same as described before. 3 weeks after the final tamoxifen injection, 1 mL 3% (w/v) thioglycolate solution (Thermo Fisher, B11716) was intraperitoneally injected. 5 days later, 10 mL ice-cold DPBS (Thermo Fisher, 14190144) was intraperitoneally injected to isolate the accumulated macrophages in the peritoneal cavity. Cells were spun down at 400 g for 10 min at 4°C for downstream analysis. Isolated cells or 30–50 mg of frozen tissues were added to bulk tubes (Thermo Fisher, 15340162) containing metal beads and 1 mL TRIzol Reagent (Invitrogen, 15596026). Tissues were then homogenized using a Benchmark BeadBlaster Homogenizer at 4°C. The mixture was spun down at 13,000 rpm for 10 min at 4°C to pellet the insoluble materials. RNA was extracted using a RNeasy Mini Kit (Qiagen, 74106) and reverse-transcribed using a High-Capacity cDNA Reverse Transcription Kit (Thermo Fisher, 4368813). Quantitative PCR was performed using Ssoadvantage Universal SYBR Green mix (Biorad, 1725272) with a CFX Opus Real-Time PCR instrument. All values were normalized by the $\Delta\Delta$ Ct method to *Rps18*. Primer sequences used are described in [key resources table](#).

Plasma and tissue sample preparation from mice

2 h after the final bout of running (time point is 4 h after the biotin intraperitoneal injection and is the same for both sedentary and exercise animals), blood was collected via submandibular bleeding using a 21G needle (BD, 305129) into lithium heparin tubes (BD, 365985) and immediately spun down at 5,000 rpm for 5 min at 4°C to retrieve the plasma fractions. All tissues were dissected, weighed on a scale, collected into Eppendorf tubes, and immediately frozen on dry ice and stored at –80°C. Adipose tissues were collected into 4% paraformaldehyde for histology analysis. For western blot analysis, tissues were mixed with 0.5 mL of cold RIPA buffer and homogenized using a Benchmark BeadBlaster Homogenizer at 4°C. The mixture was spun down at 13,000 rpm for 10 min at 4°C to pellet the insoluble materials. The supernatant was quantified using a tabletop Nanodrop One and analyzed by western blot. To remove remaining biotin from blood plasma, 200 µL plasma from a single mouse was added with 15 mL PBS and subsequently concentrated 30-fold using 3 kDa filter tubes (Millipore, UFC900324) by spinning down at 4,000 rpm for 1 h. The flowthrough was discarded, and the dilution and centrifugation steps were repeated until a final solution of 500 µL was retrieved at a 9000-fold final dilution. To enrich biotinylated plasma proteins, 200 µL Dynabeads MyOne Streptavidin T1 magnetic beads (Thermo Fisher, 65602) were washed twice with 1 mL washing buffer (50 mM Tris-HCl, 150 mM NaCl, 0.1% SDS, 0.5% sodium deoxycholate, 1% NP-40, 1 mM EDTA, 1× HALT protease inhibitor, 5 mM trolox, 10 mM sodium azide and 10 mM sodium ascorbate) and resuspended in 100 µL washing buffer. The beads were then added to the 500 µL biotin-free plasma solution and incubated at 4°C overnight with rotation. The beads were subsequently washed twice with 1 mL washing buffer, once with 1 mL 1 M KCl solution, once with 1 mL 0.1 M Na₂CO₃ solution, once with 1 mL 2 M urea in 10 mM Tris-HCl (pH 8.0), and twice with 1 mL washing buffer. Eppendorf tubes containing beads were vortexed for 3s between each step to ensure thorough washing. Finally, biotinylated proteins were eluted by boiling at 95°C for 10 min in 60 µL of 2× sample buffer supplemented with 20 mM DTT and 2 mM biotin. Successful enrichment of biotinylated plasma proteins was validated by running the elution sample on NuPAGE 4–12% Bis-Tris gels followed by silver staining (Thermo Fisher, LC6070) according to the instructions from the manufacturer's protocol.

Proteomic sample processing

After cooling down to room temperature for 3 min, boiled streptavidin-purified plasma samples (60 µL) were digested using a Mini S-Trap protocol provided by the manufacturer (Protifi, C02-micro-80). As previously described,²⁷ cysteine residues were first alkylated by incubating in 30 mM iodoacetamide (Sigma, A3221) in the dark at room temperature for 30 min. Samples were then acidified with phosphoric acid at a final concentration of 1.2%. 420 µL bind/wash buffer (100 mM tetraethylammonium bromide (TEAB) in 90% methanol) was added to each sample. 150 µL samples were loaded onto micro S-trap columns and spun down at 4000 g for 20 s. The flow-through was discarded, and the centrifugation step was repeated until all the solution passed through the column. Following four washes with 150 µL bind/wash buffer, 1 µg trypsin (Promega, V5113) was added to the S-trap and incubated at 47°C for 90 min. After trypsinization, peptides were washed once with 50 mM TEAB (40 µL), once 0.2% formic acid (40 µL), once with a mixture of 50% acetonitrile and 0.2% formic acid (40 µL) and once of 0.2% formic acid in water (40 µL) by spinning down at 1,000g for 60 s. Eluted fraction from each wash was combined, lyophilized, resuspended in 0.2% formic acid, normalized to concentration using a Nanodrop Spectrophotometer (Thermo Fisher, absorbance at 205 nm), and analyzed by LC-MS/MS. One microliter of each sample was taken and combined into a pooled sample that was used to make the chromatogram library.

Proteomics data acquisition

Proteomics data were acquired using a spectrum-library free DIA approach that relies on gas-phase fractionation (GPF) to generate DIA-only chromatogram libraries.^{38,39} Peptides were separated over a 25 cm Aurora Series Gen2 reverse-phase LC column (75 µm inner diameter packed with 1.6 µm FSC C18 particles, Ion Opticks). The mobile phases (A: water with 0.2% formic acid and B: acetonitrile with 0.2% formic acid) were driven and controlled by a Dionex Ultimate 3000 RPLC nano system (Thermo Fisher). An integrated loading pump was used to load peptides onto a trap column (Acclaim PepMap 100C18, 5 µm particles, 20 mm length, Thermo Fisher) at 5 µL/min, which was put in line with the analytical column 5.5 min into the gradient. The gradient was held at 0% B for the first 6 min of the analysis, followed by an increase from 0% to 5% B from 6 to 6.5 min, and increase from 5 to 22% B from 6.5 to 66.5 min, an increase from 22% to 90% from 66.5 to 71 min, isocratic flow at 90% B from 71 to 75 min, and re-equilibration at 0% B for 15 min for a total analysis time of 90 min per acquisition. Eluted peptides were analyzed on an Orbitrap Fusion Tribrid MS system (Thermo Fisher). Precursors were ionized with a spray voltage held at +2.2 kV relative to ground, the RF lens was set to 60%, and the inlet capillary temperature was held at 275°C.

Six chromatogram library files were collected through six repeated injections of the pooled sample only. Here, the instrument was configured to acquire 4 *m/z* precursor isolation window DIA spectra using a staggered isolation window pattern⁸⁵ from narrow mass ranges using window placements optimized by Skyline. DIA MS/MS spectra were acquired with an AGC target of 400,000 charges, a maximum injection time of 54 ms, beam-type collisional dissociation (i.e., HCD) with a normalized collision energy of 33, and a resolution of 30,000 at 200 *m/z* using the Orbitrap as a mass analyzer. The six gas-phase fractionation chromatogram libraries were collected with nominal mass ranges of 400–500 *m/z*, 500–600 *m/z*, 600–700 *m/z*, 700–800 *m/z*, 800–900 *m/z*, and 900–1000 *m/z*. The exact windowing scheme was downloaded from <https://bitbucket.org/searle/encyclopedia/wiki/Home>³⁹ and is available in [supplemental information](#) here. Precursor MS1 spectra were interspersed every 25 scans with an AGC target of 400,000 charges, a maximum injection time of 55 ms, a resolution of 60,000 at 200 *m/z* using the Orbitrap as a mass analyzer, and a scan range of either 395–505 *m/z*, 495–605 *m/z*, 595–705 *m/z*, 695–805 *m/z*, 795–905 *m/z*, or 895–1005 *m/z*.

For quantitative samples (i.e., the non-pooled samples) the instrument was configured to acquire 25 x 16 *m/z* precursor isolation window DIA spectra covering 385–1015 *m/z* using a staggered isolation window pattern with window placements optimized by Skyline (windowing scheme downloaded from the same link as above and available as [supplemental information](#) here). DIA spectra were acquired with the same MS/MS settings described above. Precursor MS1 spectra were interspersed every 38 scans with a scan range of 385–1015 *m/z*, an AGC target of 400,000 charges, a maximum injection time of 55 ms, and a resolution of 60,000 at 200 *m/z* using the Orbitrap as a mass analyzer. The detailed parameters were recorded in [Table S6](#). The mass spectrometry proteomics data have been deposited to the ProteomeXchange Consortium via the PRIDE partner repository with the dataset identifier PRIDE: PXD034535.⁸⁶

Proteomics data analysis to generate cell type-protein pairs

Staggered DIA spectra were demultiplexed from raw data into mzML files with 10 ppm accuracy using MSConvert⁸⁷ with settings described in Pino et al.³⁹ Encyclopedia (version 1.12.31)³⁸ was used to search demultiplexed mzML files using an internal PECAN fasta search engine called Walnut⁸⁸ and a reviewed-plus-isoforms mouse proteome database downloaded February 25, 2022 from Uniprot.⁸⁹ Walnut settings were: fixed cysteine carbamidomethylation, full tryptic digestion with up to 2 missed cleavages, HCD (y-only) fragmentation, 10 ppm precursor and fragment mass tolerances, and 5 quantitative ions. The chromatogram library resulting from the Walnut search was then used for Encyclopedia searching, where all similar settings to the Walnut search remained the same, and other settings included a library mass tolerance of 10 ppm, inclusion of both b- and y-type fragment ions, and a minimum number of quantitative ions set at 3. Percolator (version 3.1) was used to filter peptides to a 1% false discovery rate using the target/decoy approach and proteins to a 1% protein-level FDR assuming protein grouping parsimony. Resulting data from EncyclopeDIA were checked in Skyline⁴¹ before further processing with Perseus.⁴⁰ Proteins were filtered so that only proteins with 2 or more peptides and those that were detected in all three replicates of at least one condition were retained. Data was converted to cell type-protein pairs, and the median value of the cell type-protein pair intensity was compared to the intensity of that protein detected in WT mice control samples. Keratins were manually removed from our dataset as these proteins are frequently detectable contaminants in mass spectrometry experiments.⁹⁰ To remove background labeling contaminants, only cell type-protein pairs that showed a greater than 1.5-fold intensity above the median intensity detected in WT samples were retained.³² Then cell type-protein pairs with detected protein intensity across all 6 samples (sedentary and exercise) were included for downstream analysis. Next, cell type-protein pairs with variance >2 ($(\log_2(\text{maximum intensity}) - \log_2(\text{minimum intensity})) > 2$ under either sedentary or exercise conditions) were excluded from further analysis.⁹¹ In total, 1272 cell type-protein pairs passed the above filtering criteria and were considered as bona fide cell type-protein pairs.

Exercise responsiveness scores calculations

Exercise training-regulated cell type-protein pairs (adjusted *p*-values <0.05 and exercise fold change >1.5) were used for calculating exercise responsiveness scores. Each cell type-protein pair's exercise responsiveness was calculated as $\text{abs}(\log_{10}(\text{adjusted } p\text{-values})) \times \text{abs}(\log_2(\text{exercise fold change}))$. Exercise fold change of a cell type-protein pair was defined as median protein abundance across three exercise samples divided by median protein abundance across three sedentary samples of the same genotype. Then the exercise responsiveness scores were calculated by the summarization of the exercise responsiveness of each cell type-protein pair from the same cell type.

Time course of *Pdgfra*-cre secretomes

AAV9-FLEX-ER-TurboID virus was injected as previously described into 6-week-old hemizygous male *Pdgfra*-creER mice at a dose of 3×10^{11} GC per mouse. After a 2-week transduction period, tamoxifen was delivered to induce cre-mediated expression of ER-TurboID. Three weeks after the final tamoxifen injection, mice were divided into three groups (1-day running, 3-day running, 7-day running and sedentary controls, $n = 3/\text{condition}$). 1 h before the last bout of running, biotin was administered by injection (24 mg/mL, intraperitoneally, in a solution of 18:1:1 saline:Kolliphor EL:DMSO, final volume of 400 μL per mouse per day). The treadmill running was carried out as previously described. For the 1-day running group, mice were sacrificed, and blood and tissue samples were analyzed 2 h after a single bout of running. For 3-day or 7-day running groups, mice were run for 3 or 7 consecutive days and blood and tissues were harvested 2 h after the final bout of running. For the sedentary group, biotin was administered, and blood and tissue samples were collected 4 h after biotin delivery.

Gene ontology analysis

Proteins with adjusted *p*-values <0.05 and exercise fold change >1.5 from *Pdgfra* secretomes were uploaded to online gene ontology analysis tool <http://geneontology.org/>.⁹² The enriched biological processes were ranked by gene ratio and *p*-values.

Isolation and culture of primary mouse hepatocytes

Primary mouse hepatocytes were isolated and cultured as previously described.^{28,93} Briefly, 8 to 12-week-old male mice (C57BL/6J) were sacrificed and perfused with perfusion buffer (1 g/L glucose, 2.1 g/L sodium bicarbonate, 0.4 g/L potassium chloride and 0.2 g/L EDTA in HBSS buffer) via cannulate vena cava for 5 to 8 min and then with digestion buffer (1 mg/mL collagenase IV (Sigma, C5138-1G) in DMEM/F-12 medium) for 5 to 8 min. The liver was then dissected out, cut into small pieces using a razor blade and passed through a 70- μm cell strainer (BD, 352350) to obtain crude hepatocytes. Cells were then spun down at 50 g for 3 min, resuspended

in 10 mL plating medium (10% FBS, 1 μ M dexamethasone (Sigma, D4902-100MG), 0.1 μ M insulin (Sigma, 91077C), 2 mM sodium pyruvate, 1% penicillin–streptomycin in William's E medium (Quality Biological, 10128-636)) and spun down again at 50 g for additional 3 min. The pellet was resuspended in 10 mL of a 45% Percoll solution in PBS and spun down at 100 g for 10 min to isolate hepatocytes. The final hepatocyte pellet was resuspended in 10 mL plating medium, spun down again at 50 g for 5 min and resuspended in 1 mL plating medium. Cells were counted and plated in a collagen-coated six-well plate at 2 million cells per well. 4 h later, the plating medium was changed to warm maintenance medium (0.1 μ M dexamethasone, 1 nM insulin, 0.2% BSA (Sigma, A7906-500G), 2 mM sodium pyruvate, 1% penicillin–streptomycin), and cells were incubated overnight before further treatment.

Treatment of hepatocytes with organic compounds, MCT inhibitor and brefeldin A

24 h after plating, primary hepatocytes were washed twice with warm PBS to remove BSA. Then 2 mL William's E medium containing the indicated concentrations of sodium lactate (Sigma, 05508-5ML), 2 mM sodium fumarate dibasic (Sigma, F1506-25G), 2 mM sodium succinate dibasic hexahydrate (Sigma, S2378-100G), 2 mM sodium (R)-3-hydroxybutyrate (Sigma, 298360-1G), 2 mM kynuronic acid (Sigma, K3375-250MG), 2 mM D-Pantothenic acid hemicalcium salt (Sigma, 21210-5G-F), 2 mM sodium pyruvate (Sigma, P2256-25G), 2 mM L-(–)-Malic acid (Sigma, 02288-10G) was added. The above organic compounds powder was dissolved in ethyl alcohol 200 proof to make 100 mM master stock and diluted accordingly to reach the indicated concentration in medium. 40 μ L ethanol was added as negative control. For MCT inhibitor AR-C155858 (Tocris, 4960) and Brefeldin A (Sigma, B6542-5MG), compound power was dissolved in DMSO to make master stock (100 μ M for AR-C155858 and 5 mg/mL for Brefeldin A) and diluted accordingly to reach the indicated concentration in medium containing 2 mM sodium lactate. 4 h later, cells and conditioned medium were harvested and analyzed by western blotting as previously described. For HEK293T cells, cells were washed twice with warm PBS 24 h after transfection and incubated with serum-free medium containing indicated concentration of sodium lactate. 4 h later, cells and conditioned medium were harvested and analyzed by western blotting as described above.

Construction of plasmids for overexpression of CES2A/C- Δ C

Flag-CES2A- Δ C fragment (ref sequence NM_133960.5) and Flag-CES2C- Δ C fragment (ref sequence NM_145603.2) were synthesized as gBlocks with IDT. For both fragments, 5'-GACTACAAGGATGACGACGATAAGGGGGCGGT-3' sequences (encoding FLAG tag) were inserted after CES2 sequences encoding secretory signal peptide (1–78 nt). For Flag-CES2A- Δ C fragment, C-terminal 5'-CATGCAGAGCTG-3' sequences (encoding HAEL as ER retention signal peptide) were deleted. For Flag-CES2C- Δ C fragment, C-terminal 5'-CACAGGGAGCTT-3' sequences (encoding HREL as ER retention signal peptide) were deleted. Both gene fragments were inserted into D-TOPO vector using pENTR/D-TOPO Cloning Kit (Invitrogen, K240020) and shuttled into pDEST40 mammalian expression vector using Gateway LR Clonase Enzyme mix (Invitrogen, 11791019). The pDEST40 plasmids were then transformed into One Shot TOP10 Chemically Competent *E. coli* (Invitrogen, C404010), extracted and sequence verified. pAAV-*Tbg*-ER-TurboID plasmid (Addgene, 149415) was cut with restriction enzymes NotI and HindIII to generate the backbone vector. Flag-CES2A- Δ C fragment was amplified using primer sets: 5'-TGCCTTTCTCTCCACAGGTGTCCAGGCGCCGCGCCACCATGCCATTGGCTAGACTTC-3', 5'-CCAGAGGTTGATTGGATCCAAGCTTCTACTTGTCTCTGAGAACCCTTGAGCTCCTG-3'. Flag-CES2C- Δ C fragment was amplified using primer sets: 5'-TGCCTTTCTCTCCACAGGTGTCCAGGCGCCGCGCCACCATGACACGGAACCACTACATAAC-3'; 5'-CCAGAGGTTGATTGGATCCAAGCTTCTACTTGTCTCTGAGAAGCCTTTAGCTCCTGG-3'. Both PCR products were purified using QIAquick gel extraction kit (Qiagen, 28704) and ligated with the linearized pAAV-*Tbg* vector using Gibson Assembly Master Mix (NEB Biolabs, E2611L). Ligated plasmids were transformed into One Shot TOP10 Chemically Competent *E. coli* (Invitrogen, C404010), extracted and sequence verified. pDEST40-Flag-CES2A- Δ C-S227A and pDEST40-Flag-CES2C- Δ C-S230A plasmids were generated with pDEST40-Flag-CES2A- Δ C and pDEST40-Flag-CES2C- Δ C as the templates respectively using Q5 Site-Directed Mutagenesis Kit (NEB Biolabs, E0554S). Flag-CES2A- Δ C-S227A and Flag-CES2C- Δ C-S230A fragments were amplified, purified and inserted into pAAV-*Tbg* vector as previously described.

Generation of recombinant CES2 proteins

Recombinant CES2A and CES2C proteins were generated by transient transfection of pDEST40-CES2A/C- Δ C, pDEST40-CES2A- Δ C-S227A, pDEST40-CES2C- Δ C-S230A plasmids in mammalian Expi293 cells following the manufacturer's instructions. Five to seven days after transfection, conditioned medium was collected, and recombinant proteins were purified using a His GraviTrap TALON column and buffer exchanged to PBS. Protein purity and integrity were analyzed by SDS page. Following purification, recombinant proteins were aliquoted and stored at -80°C to avoid freeze-thaws.

Determination of CES2A- Δ C and CES2C- Δ C secretion in cell culture

HEK293T cells were transfected as described above. 30 h after transfection, cells were washed twice with PBS and added with 10 mL serum-free medium. 12 h later, conditioned medium (10 mL) was collected and concentrated 20-fold using 10 kDa filter tubes (Millipore, UFC801024) to 500 μ L. Concentrated conditioned medium was mixed with 4 \times loading buffer (NuPAGE LDS Sample Buffer, Invitrogen, NP0008, 100 mM DTT) and boiled for 10 min at 95°C . Cells were collected and lysed by probe sonication in RIPA buffer (1% NP-40, 0.1% SDS, 0.5% sodium deoxycholate and 1:100 HALT protease inhibitor, Thermo Fisher, 78429) for 1 min. Cell lysates were spun down at 13000 rpm for 10 min at 4°C . The supernatant was collected, quantified using a tabletop Nanodrop One, boiled for 10 min at 95°C . Both conditioned medium and cell lysate samples were then analyzed by western blot.

Histology

Adipose tissues were collected into 4% paraformaldehyde and fixed at 4°C with rotation for 72 h. Fixing solution was replaced with 20% sucrose solution. Adipose tissues were dehydrated for additional 24 h before freezing in OCT-embedded block (Thermo Fisher, 23-730-571) and cryosectioned. H&E staining was conducted on the slides by Stanford Animal Histology Core.

Glucose tolerance and insulin tolerance tests in mice

For glucose tolerance tests, mice were fasted for 6 h (fasting starting 8 a.m. in the morning) and then intraperitoneally injected with glucose at 2 g/kg body weight. Blood glucose levels were measured at 0, 20, 40, 60, and 120 min via tail bleeding using a glucose meter. For insulin tolerance tests, mice were fasted for 6 h (fasting starting 8 a.m. in the morning) and then intraperitoneally injected with insulin in saline 0.75 U/kg body weight. Blood glucose levels were measured at 0, 20, 40, 60, and 120 min via tail bleeding using a glucose meter.

Maximal running capacity test

8 weeks after viral transduction, mice were acclimated to the treadmill two days prior to the maximal running tests (10 min at 10 m/min). The maximal running test was performed as previously described.^{67,68} Briefly, running started at 9.6 m/min with 14.5° incline for 60 s, followed by a continuous increase (1.2 m/min) in running speed every 60 s until exhaustion. The test was randomized where each experimental group ran on different lanes of the treadmill. In addition, the test was also performed blinded (one person placing the mice on the treadmills, another person (blinded) to determine the exhaustion of the individual mouse).

Chronic treadmill running

8 to 10-week-old male C57BL/6 mice were injected with AAV8-*Tbg*-CES2A/C- Δ C/GFP viruses via tail vein at a dose of 10e11 GC per mouse. One week after viral transduction, mice were fed with HFD (60% fat, Research Diets, D12492) for 4-week. Then mice Body weights and food intake were measured every week. Starting from the fifth week, mice were subjected to treadmill running daily (5 days per week) for 4 consecutive weeks. Mice were acclimated to the treadmill for 5 min before running at a speed of 5 m/min for 5 min. Then the speed was increased to 15 m/min and kept constant for 60 min. A serological pipette was used to manually stir the mice to avoid excessive electrical shock during the whole running period. After exercise training, mice were returned to home cages. The sedentary control animals were kept in their home cages but removed from the original racks and put next to the treadmill. These mice were constantly disturbed by the noises from the running animals and treadmill and therefore were kept awake during the whole duration of the running of the exercise animals. Running was performed for 5 consecutive days in the morning (between 9 and 12 a.m.) per week followed by 2-day rest.

Indirect calorimetry and physiological measurements

8 to 10-week-old male C57BL/6 mice were injected with AAV8-*Tbg*-CES2A/C- Δ C/GFP viruses via tail vein at a dose of 10¹¹ GC per mouse. One week after viral transduction, mice were fed with HFD (60% fat, Research Diets, D12492). Body weights and food intake were measured every week. Before the body weights of AAV8-*Tbg*-CES2A/C- Δ C injected mice started to be significantly different from AAV8-*Tbg*-GFP injected mice (~3 weeks for AAV8-*Tbg*-CES2C- Δ C and ~5 weeks for AAV8-*Tbg*-CES2A- Δ C), metabolic parameters including oxygen consumption, respiratory exchange ratio, food intake and movement of mice were measured using the environment-controlled home-cage CLAMS system (Columbus Instruments) at the Stanford Diabetes Center. Mice were housed in the metabolic chambers for 24 h prior to the start of experiment. Energy expenditure calculations were normalized for body weight. *p*-values were calculated from two-way ANOVA.

LC-MS detection of blood plasma lactate

10 to 12-week old male C57BL/6 mice were subjected to 1-week treadmill running protocol used in this experiment. The sedentary control animals were kept in their home cages but removed from the original racks and put next to the treadmill. These mice were constantly disturbed by the noises from the running animals and treadmill and therefore were kept awake during the whole duration of the running of the exercise animals. The exercise mice were sacrificed immediately after the last bout of running and blood plasma was harvested and processed as previously described. Then 150 μ L of a 2:1 mixture of acetonitrile:methanol was added to 50 μ L of plasma to extract polar metabolites. The mixture was then spun down at 13,000 rpm for 10 min at 4°C and the supernatant was transferred to an LC-MS vial for analysis using an Agilent 6470 triple quadrupole LC-MS instrument. Separation of polar metabolites was conducted as previously described (Lac-phe paper). Briefly, a Luna 5 μ m NH₂ 100 Å LC column (Phenomenex 00B-4378-E0) was used for LC with normal phase chromatography. Mobile phases compositions were as follows: buffer A, 95:5 water:acetonitrile with 0.2% ammonium hydroxide and 10 mM ammonium acetate; buffer B, acetonitrile. The LC gradient started at 100% buffer B with a flow rate of 0.7 mL/min from 0 to 2 min. The gradient was then linearly increased to 50% A/50% B at a flow rate of 0.7 mL/min from 2 to 20 min. From 20 to 25 min, the gradient was maintained at 50% A/50% B at a flow rate of 0.7 mL/min. Finally, 100% buffer B was maintained at a flow rate of 0.7 mL/min for 5min to equilibrate the column. MS analysis was performed in negative mode using ESI. The AJS ESI source parameters were set as follows: the capillary voltage was set to 3,500 V; the sheath gas temperature was set to 300°C with the sheath gas flow set at 12 L/min; and the gas temperature was set at 250°C with a gas flow of 12 L/min and the nebulizer pressure was at 25 psi. Quantification of the plasma lactate concentrations were performed by generating a standard curve with known concentrations of sodium lactate. Lactate standards were analyzed using the same targeted method and

run on the same batch and a standard curve was generated from the lactate concentrations and total ion intensities were used to calculate the plasma lactate concentrations.

Untargeted metabolomics by LC-MS

12 to 16-week old male C57BL/6 mice ($n = 5/\text{group}$) transduced with AAV-*Tbg*-CES2A- ΔC , AAV-*Tbg*-CES2C- ΔC or AAV-*Tbg*-GFP. Untargeted metabolomics measurements were then performed as previously described.⁹⁴ Briefly, an Agilent 6520 Quadrupole time-of-flight LC-MS instrument was used for analysis. MS runs were performed using electrospray ionization (ESI) in negative mode. The dual ESI source parameters were set as follows: the gas temperature was set at 250°C with a drying gas flow of 12 L/min and the nebulizer pressure at 20 psi; the capillary voltage was set to 3,500 V; and the fragmentor voltage was set to 100 V. A Luna 5 μm NH2 100 Å LC column (Phenomenex 00B-4378-E0) with normal phase chromatography was used to separate polar metabolites. Mobile phases and LC parameters were the same as the lactate quantification LC-MS runs described above. Differential peak identification was performed with XCMS.⁹⁵

Carboxylesterases enzymatic activity measurement

A continuous spectrophotometric assay was performed using 4-nitrophenyl acetate (Sigma, N8130-5G) as substrate as previously described.⁹⁶ Briefly, 1 mM 4-nitrophenyl acetate was prepared freshly in 50 mM Tris·Cl buffer (pH 7.4). 150 μL of 4-nitrophenyl acetate solution was added into a single well of a 96-well plate (Thermo Fisher, 125565501), followed by pre-incubating 5 min at 37°C in the absorbance plate reader. 15 μg liver lysates or 3 μL plasma were diluted in 50 mM Tris·Cl buffer (pH 7.4) and added to 4-nitrophenyl acetate solution (total volume 300 μL). The formation of *p*-nitrophenolate was measured every 30 s at 405 nm for 5 min. Subtracted from background absorbance, absorbance at each time point was used to generate a kinetic plot for each sample. Data points within the linear range of the reaction were used to calculate the slope of the enzymatic reaction. Finally, relative enzymatic activity was calculated comparing the slopes of reaction from each sample.

QUANTIFICATION AND STATISTICAL ANALYSIS

Data representation and statistical analysis

All values in figures are shown as mean \pm SEM. The number of biological replicates (N) is described in each figure legend (N corresponds to the number of animals used under each condition for animal experiments and corresponds to the number of independently conducted experiments for cellular experiments). For animal studies, mice were randomly assigned to control and treatment groups. Each animal study was repeated at least twice using separate cohorts of mice. To identify statistically changed cell type-protein pairs (exercise vs. sedentary, $n = 3/\text{protein}/\text{condition}/\text{genotype}$), protein intensities were first scaled by the `scale()` function in R package.⁹⁷ The Limma package^{98,99} was implemented to conduct the moderated t-statistics¹⁰⁰ (<https://github.com/leolove2022/ModeratedtTest.git>), and adjusted p-values of each cell type-protein pair were generated into excel files. 256 cell type-protein pairs out of total 1272 pairs were defined as under exercise training regulation (adjusted p-values <0.05 and exercise fold change >1.5). Each *in vitro* experiment using primary cells from mice was repeated using at least three cohorts of mice. Two-tailed, unpaired Student's *t* test was used for single comparisons assuming the sample groups exhibited a normal distribution and comparable variance. two-way ANOVA with post hoc Sidak's multiple comparisons test with repeated measures was used for the body weights, glucose tolerance test and insulin tolerance test studies. Unless otherwise specified, statistical significance was set at adjusted p-value <0.05 for the proteomics data, and p-value <0.05 for all other comparisons.